TECHNICAL MEMORANDUM

781

# Momentum transport in shallow convection

L. Schlemmer[1,2], P. Bechtold[1], I. Sandu[1], M. Ahlgrimm[1]

Research Department

[1]ECMWF, Reading, UK,[2]ETH Zurich, Institute for Atmospheric and Climate Science, Zurich, Switzerland

August 26, 2016



European Centre for Medium-Range Weather Forecasts
Europäisches Zentrum für mittelfristige Wettervorhersage
Centre européen pour les prévisions météorologiques à moyen terme

Series: ECMWF Technical Memoranda

A full list of ECMWF Publications can be found on our web site under:
http://www.ecmwf.int/en/research/publications

Contact: library@ecmwf.int



European Centre for Medium-Range Weather Forecasts
Shinfield Park, Reading, RG2 9AX, England

**Abstract**

The vertical transport of horizontal momentum by convection has an important impact on the general circulation of the atmosphere as well as on the life cycle and track of cyclones. So far it has mostly been studied for deep convection, whereas little is known about its properties and importance in shallow convection. In this study convective momentum transport by shallow convection is investigated by analysing both data from large-eddy simulations (LES) and simulations performed with the Integrated Forecasting System (IFS) of the European Centre for Medium-Range Weather Forecasts (ECMWF). Thereby the IFS is run in 3D mode as well as in a single column model (SCM) version. In addition, the central terms underlying the bulk mass-flux parametrisation of the IFS convection scheme are evaluated offline. The analysed cases exhibit shallow convective clouds developing within considerable low-level wind shear. Analysis of the momentum fluxes in the LES data reveals significant momentum transport by the convection in both cases, which is directed down-gradient despite substantial organisation of the cloud field. A detailed inspection of the convection parametrisation reveals a very good representation of the underlying entrainment and detrainment rates and an appropriate representation of the convective mass and momentum fluxes. To determine the correct values of mass-flux and in-cloud momentum at the cloud base in the parametrisation yet remains challenging.

# 1 Introduction

Cumulus convection transports heat and moisture as well as momentum up- and downwards. Especially in flows that exhibit strong vertical wind shear such as the trade-wind region the vertical displacement of air with different horizontal momentum from lower to upper levels is a crucial process that contributes to the overall momentum budget. Observational studies (e.g. LeMone 1983) document the transport of momentum by organised convective systems. Carr and Bretherton (2001) have investigated convective momentum transport (CMT) as a momentum budget residual in reanalysis data and found a significant contribution from the residual to the budget below 850 hPa, speculating that it results from momentum transport by shallow convection. Tung and Yanai (2002a,b) have analysed the budget residual for the Tropical Ocean and Global Atmosphere Coupled Ocean-Atmosphere Response Experiment (TOGA-COARE) intense observing period. They found a link between deep cumulus convection and the acceleration-deceleration of the large-scale horizontal motion, via CMT, which was being modulated by various atmospheric disturbances. Moreover, they identified that CMT may either be up- or down-gradient, depending on the organisation of convection. For unorganised convection, CMT tends to be down-gradient, meaning that it decreases the wind shear. For organised convective systems CMT can become up-gradient and accelerate the mean flow, which has especially been documented for the line-normal direction in squall lines (LeMone 1983). Moreover, CMT can influence the track of cyclones (Hogan and Pauley 2007).

A fair amount of work has been devoted to include CMT into parametrization schemes for convection (e.g. Schneider and Lindzen 1976; Kershaw and Gregory 1997; Gregory et al. 1997; Gregory and Miller 1989) within the mass-flux framework. The critical aspect in these calculations is the treatment of the pressure-gradient (Zhang and Cho 1991). Zhang and McFarlane (1995); Inness and Gregory (1997); Wu et al. (2007) demonstrated that the mean climate in global climate simulations critically depends on the inclusion of CMT. While convective momentum transport and its parametrisation has been studied a fair amount for deep convection (e.g. Grubišić and Moncrieff 2000; Zhang and Wu 2003), little is documented about its importance in shallow convection, and its representation in parametrisation schemes. In contrast to deep convection, which is partly resolved, shallow convection shows considerably less organisation and remains a sub-grid scale process, even in present-day resolutions of Numerical Weather

Prediction (NWP) models of $\mathcal{O}(10\,\text{km})$. Brown (1999) used Large Eddy Simulations (LES) to investigate the influence of shear on CMT in shallow convection for cases of down-gradient transport. It is not clear, how well parametrisations capture CMT in shallow convection, partly due to uncertainties concerning the representation of the pressure gradient across updraughts. Moreover, the applicability of the mass-flux approximation to CMT has recently been questioned (Zhu 2015), as shear-driven small-scale eddies are more efficient in transporting momentum as coherent convective plumes.

The current study will analyse CMT in LES simulations of shallow convection in a case of trade-wind cumulus that start to organise strongly, and a cold-air outbreak case. The extracted momentum fluxes will be compared to those produced by the IFS parametrisation scheme for convection. Moreover, the underlying terms of the convection schemes will be recalculated offline from LES data to pin down the largest error sources. First, the LES data and the model used will be introduced (section 2). In section 3, the momentum fluxes and the underlying terms will be analysed and compared with the LES data. Finally, a discussion and conclusion of the results will be given in section 4.

# 2 Set-up

## 2.1 LES data

### *2.1.1 RICO*

The LES data-set used is documented in Seifert et al. (2015). Simulations were performed using the University of California, Los Angeles (UCLA) Large Eddy Simulation (LES) model (see Stevens et al. 2005). The UCLA-LES solves the 3-dimensional Ogura-Phillips anelastic equations, where one assumes an isentropic background state. The prognostic variables are the three components of the wind velocity ($u$, $v$, and $w$), the total water mixing ratio $q_t$, the liquid water potential temperature $\theta_l$ and the microphysical species. The UCLA-LES uses a third-order Runge-Kutta scheme for the time integration, a fourth order centred scheme for the advection of momentum and a flux-limited fourth order upwind scheme for the advection of scalars. A Smagorinsky-type scheme is employed to represent subgrid-scale (sgs) mixing. Surface fluxes of heat and moisture are calculated employing similarity theory given a fixed sea-surface temperature. Cloud microphysical processes are parametrised based on the two-moment warm rain scheme of Seifert and Beheng (2001) with some simplifications and refinements detailed in Stevens and Seifert (2008).

The simulations follow the GEWEX Cloud System Study (GCSS) RICO (Rain in Cumulus over the Ocean) model inter-comparison study (vanZanten et al. 2011). The domain size contains $2048x2048x200$ grid points, to span a simulated volume of $51.2\,\text{km}x51.2\,\text{km}x5\,\text{km}$. The grid is isotropic with a grid spacing of $\Delta x$=25 m and has double periodic lateral boundary conditions. We use their "rico, N070" simulation. This data represents a case of shallow trade-wind cumuli. The peculiarity of the simulations lies in the organisation of the shallow convection from random clouds into larger systems during the course of the simulation (see e.g. Fig. 2 in Seifert et al. 2015). It is thus useful for studying CMT across different organisation states of shallow convection. We pick four selected time steps for our analysis, namely 10, 20, 40 and 60 h into the simulation to sample different states of organisation. The exceptionally large domain and multitude of simulated clouds yield a large sample for the conducted analysis.

### 2.1.2 *CONSTRAIN*

The setup for the cold-air outbreak follows the case study described in Field et al. (2014). It is based on observations taken during the Met Office CONSTRAIN campaign and associated NWP simulations. Observations show that this day was characterised by northerly flow and stratocumulus clouds at 66 N -11 W. As cold air is advected over warmer sea the stratocumulus transitions to mixed-phase cumulus clouds at around 60 N, prior to reaching land. Moreover, the flow shows a strong northerly component with significant wind shear indicating a highly baroclinic situation. Cold-air outbreaks occur frequently (Brümmer and Pohlmann 2000) and influence the air-sea exchange of momentum, heat and moisture considerably (e.g. Nowlin Jr. and Parker 1974).

Simulations are performed using the UCLA-LES. In contrast to the RICO simulations a two-moment ice-microphysics scheme including ice, snow, graupel and hail as cold species developed by Seifert and Beheng (2006) is used. Radiative fluxes are calculated interactively using the "correlated-$k$" method, whereas radiative transfer is approximated utilizing a $\delta$-four stream method (Fu and Liou 1993; Pincus and Stevens 2009).

The setup and the forcing data for the LES simulations is documented at `http://appconv.metoffice.com/cold_air_outbreak/constrain_case/crm_setup.html`. The simulation uses a grid spacing of $\Delta$x=250 m in the horizontal and a stretched grid in the vertical with a minimum grid spacing of $\Delta$z = 25 m. The domain spans $96\times96\,\mathrm{km}^2$ in the horizontal and 168 levels up to 4980 m in the vertical. The roughness length for momentum is set to $6.6\times10^{-4}$ m and the roughness length for scalars to $3.7\times10^{-6}$ m. A time-varying sea-surface temperature (SST) is prescribed to mimic the southward advection of the domain. In contrast to the setup proposed in Field et al. (2014), the initial values of $u$ and $v$ are used as the geostrophic winds $u_g$ and $v_g$, respectively. The simulation is run for 14.5 h. The first 1.5 h are considered as spin up period.

## 2.2 3D IFS

To analyse the representation of CMT in the Integrated Forecast System (IFS) of the European Centre for Medium-Range Weather Forecasts (ECMWF), global Numerical Weather Prediction (NWP) integrations have been performed using version CY42R1 at a resolution of T1279 with 137 levels in the vertical. The RICO case simulations are started from ERA-INTERIM and run as short-term forecasts with a lead time of 48 h. Forecasts cover the period December 16, 2004, 00 UTC until January 8th, 2005, 00 UTC which corresponds to the undisturbed period of the RICO campaign. Simulations for the CONSTRAIN case are started from the operational analysis and run for 36 h over the period January 30, 2010, 12 UTC to February 1st, 2010, 00 UTC.

While the IFS simulation retrieved for the CONSTRAIN case was very useful for a comparison with the LES data, the RICO run turned out to be rather different from the LES case, which represents the equilibrium state of the trade-wind cumulus area. The RICO run was thus discarded for further analyses. For the comparison of the IFS with the LES a domain that follows the LES track moving southward is extracted from the global IFS data for the CONSTRAIN case. It covers an area of $1^\circ \times 1^\circ$ and its centre point is located at 66°N, 11°W at 00 UTC on January 31, 2010. The domain is moved at a constant speed to 60°N, 8.7°W at 13 UTC on January 31, 2010.

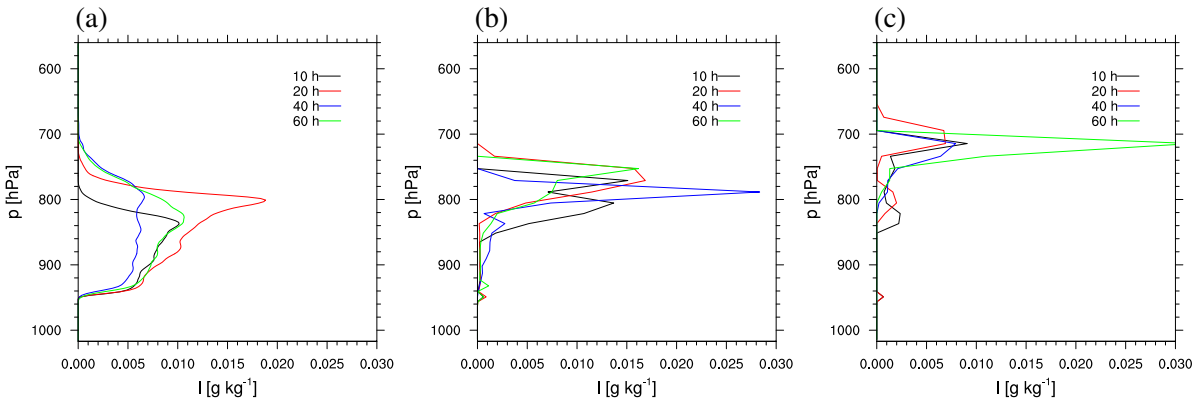


*Figure 1: Liquid water content ($g\,kg^{-1}$) at the different times of analysis in (a) the LES data, (b) the SCM and (c) the SCM_new runs.*

## 2.3 SCM

In order to compare the IFS more directly with the LES data, in addition a single-column model (SCM) version of the IFS has been run. The SCM is based on IFS version CY41R1. These runs will be labelled "SCM" in the following. A further set of simulations with an updated version of the SCM is run. The modifications to the convection routine of this updated version is the introduction of an absolute mass flux limit of $2\,kg\,m^{-2}\,s^{-1}$ and modifications to the closure for shallow convection. These runs will be denoted "SCM_new" in the following.
The SCM is run equivalently to a resolution of T1279L137 using a time step of 900 s.

### *2.3.1 Short RICO runs*

Short SCM simulations, spanning 11 time steps are run starting from domain-mean profiles extracted from the RICO LES datasets. A relaxation towards the initial profile with a time constant of 7200 s is applied to keep the simulated profiles close to the initial ones. The output averaged over time steps 2-11 is used to compare quantities simulated by the SCM with the LES. This strategy enables a direct comparison between SCM and LES data.

### *2.3.2 CONSTRAIN*

The SCM was run using the initial data and large-scale forcing for the LES CONSTRAIN case. The simulation spans 14.5 h and the first 1.5 h serve as spin up. Simulated fields are relaxed to the fields provided for the intercomparison case (simulated by the UM LAM) with a time constant of 7200 s.

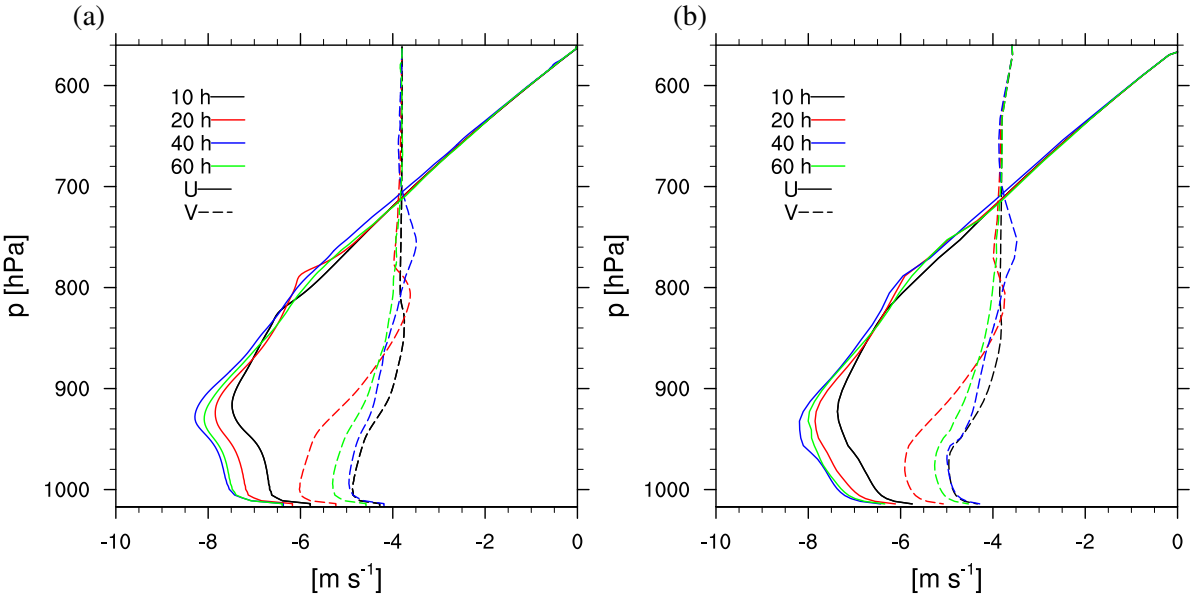


*Figure 2: Zonal (solid) and meridional (dashed) wind ($m\,s^{-1}$) at the different times of analysis in (a) the LES data and (b) the SCM runs.*

# 3 Results

## 3.1 RICO

### *3.1.1 Overview*

Figure 1 shows the domain mean liquid water content for the different analysis times of the LES, as well as those recalculated using the short SCM runs. Between hour 10 and hour 20 liquid water content increases, and shows an increase with height in the LES. As clouds start to organise, domain mean liquid water decreases again and the cloud top shifts downwards. Feeding the profiles extracted at those time steps into the SCM results in a very similar magnitude of the liquid water content, whereas the profiles are shifted upwards, and the SCM tends to deposit the water in the upper part of the clouds. In the SCM_new simulations the liquid water content decreases and is even more located in the upper parts of the clouds.

The zonal wind exhibits strong shear decreasing from values as low as -8 $m\,s^{-1}$ at cloud base to 0 $m\,s^{-1}$ at the LES model top (Fig. 2). In the sub-cloud layer the zonal wind decreases towards -6 $m\,s^{-1}$. The meridional wind is more or less constant with height, with a slight increase in the sub-cloud layer and decreasing values directly at the surface. This patterns is consistent within the LES and the SCM runs. Moreover, a similar flow structure with a low-level jet in the zonal wind, and a more or less constant profile in the meridional wind is found in ERA-INTERIM (not shown). The pattern remains constant over time, with a slight increase of the wind shear towards later times of the simulation. Thus, the momentum is affected little by the cloud organisation. We will focus on hour 10 (unorganised state) and hour 60 (organised state) in the following.

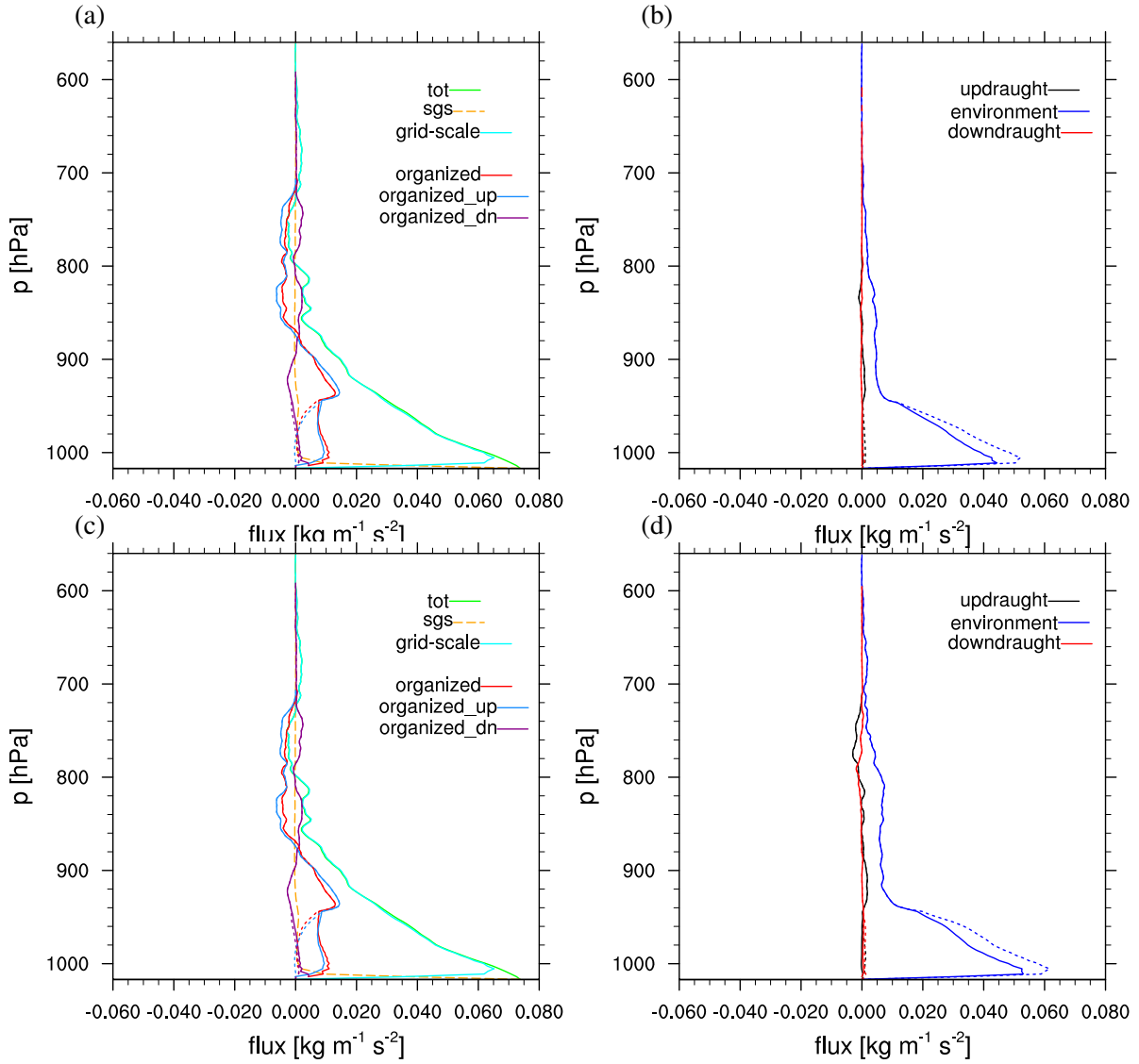


*Figure 3: Total (green), sub-grid scale (orange dashed line) and grid-scale (cyan) vertical flux of zonal momentum ($kg\,m^{-1}\,s^{-2}$) in the LES at (a) 10 h and (c) 60 h. The total organised vertical flux of zonal momentum ($kg\,m^{-1}\,s^{-2}$, cf. Eq. 1) as recomputed from the LES data (red) is further split up into the updraught (blue) and downdraught (violet) contribution. Panels (b) and (d) show the updraught (black), environment (blue) and downdraught (red) components (cf. Eq. 1) of the vertical flux as recomputed from the LES at (a) 10 h and (c) 60 h.*

### *3.1.2 Analysis of the parametrised terms*

The large high-resolution LES data set offers the possibility to evaluate the quantities and terms involved in the IFS parametrisation in detail. This is achieved by computing the terms under scrutiny form the LES data and either comparing directly with the IFS output, or additionally inserting certain LES derived quantities directly in the IFS parametrization and recomputing the remaining terms/quantities. The latter approach allows to assess more directly the uncertainty of the whole parametrization framework and uncertainties related to specific terms in the parametrization.

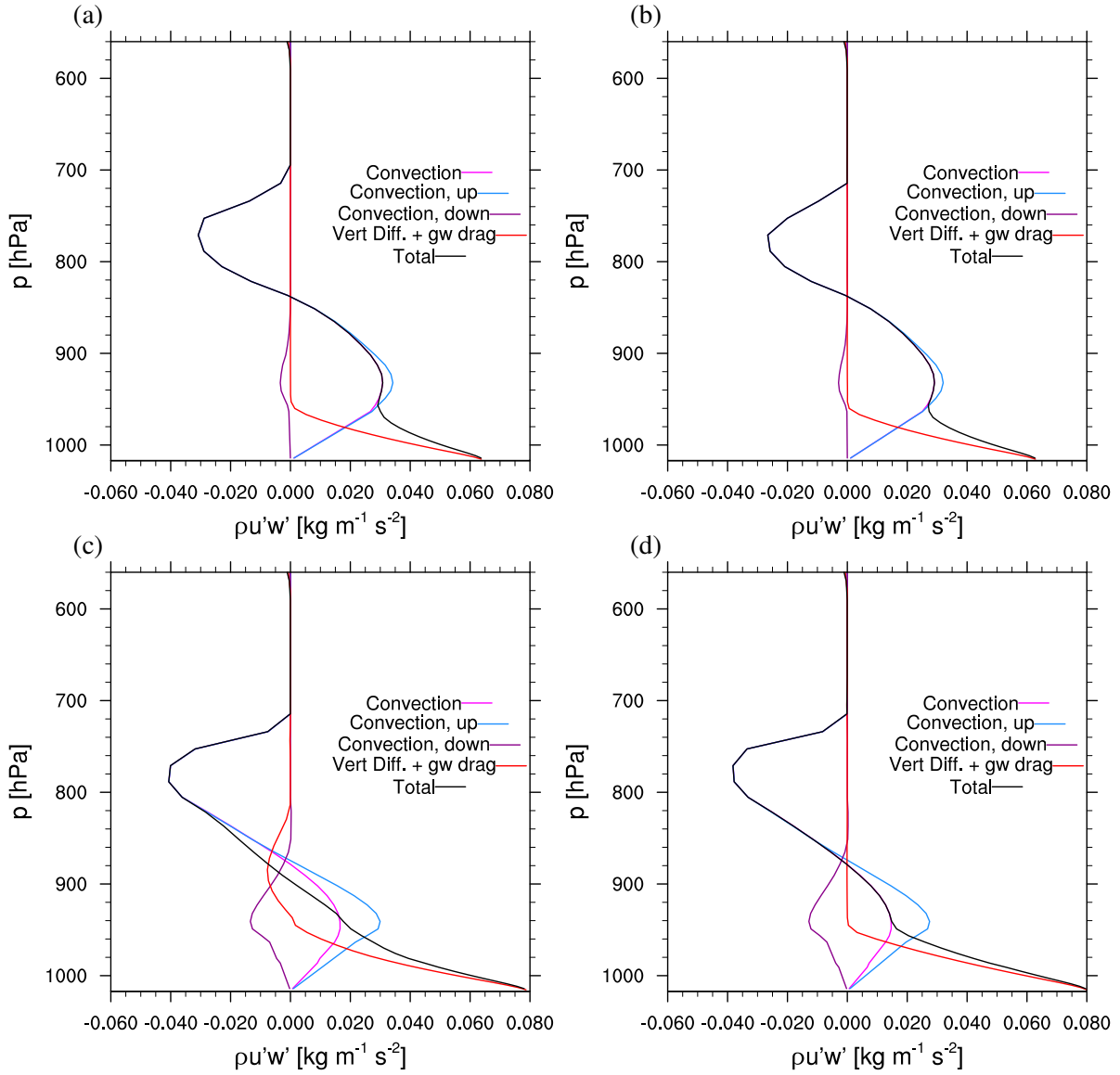


*Figure 4: Different contributions to the vertical flux of zonal momentum (kg $m^{-1}$ $s^{-2}$) in the SCM runs at (a, c) and the SCM_new (b, d) runs at 10 h (upper row) and 60 h (lower row). The total momentum flux from the convection routine (magenta) is split up into the updraught (blue) and downdraught (violet) contribution.*

**Momentum fluxes** In the IFS model cumulus convection is parametrised using a bulk mass-flux scheme (Tiedtke 1989). The mass-flux approach which was first pioneered by Arakawa and Schubert (1974) decomposes the vertical flux $\overline{w'\chi'}$ of a variable $\chi$ into multiple terms:

$$\overline{w'\chi'} = \underbrace{\sigma_u \overline{w''\chi''}^u}_{\text{updraught}} + \underbrace{\sigma_d \overline{w''\chi''}^d}_{\text{downdraught}} + \underbrace{(1-\sigma_u-\sigma_d)\overline{w''\chi''}^e}_{\text{environment}} + \underbrace{\sigma_u(\overline{w}^u-\overline{w})(\overline{\chi}^u-\overline{\chi}) + \sigma_d(\overline{w}^d-\overline{w})(\overline{\chi}^d-\overline{\chi}) + (1-\sigma_u-\sigma_d)(\overline{w}^e-\overline{w})(\overline{\chi}^e-\overline{\chi})}_{\text{organised}} \quad (1)$$

where $\sigma_u$ and $\sigma_d$ are the updraught and downdraught fraction, respectively, and $w$ is vertical velocity. Primed variables indicate deviations with respect to the domain mean values, whereas double primes

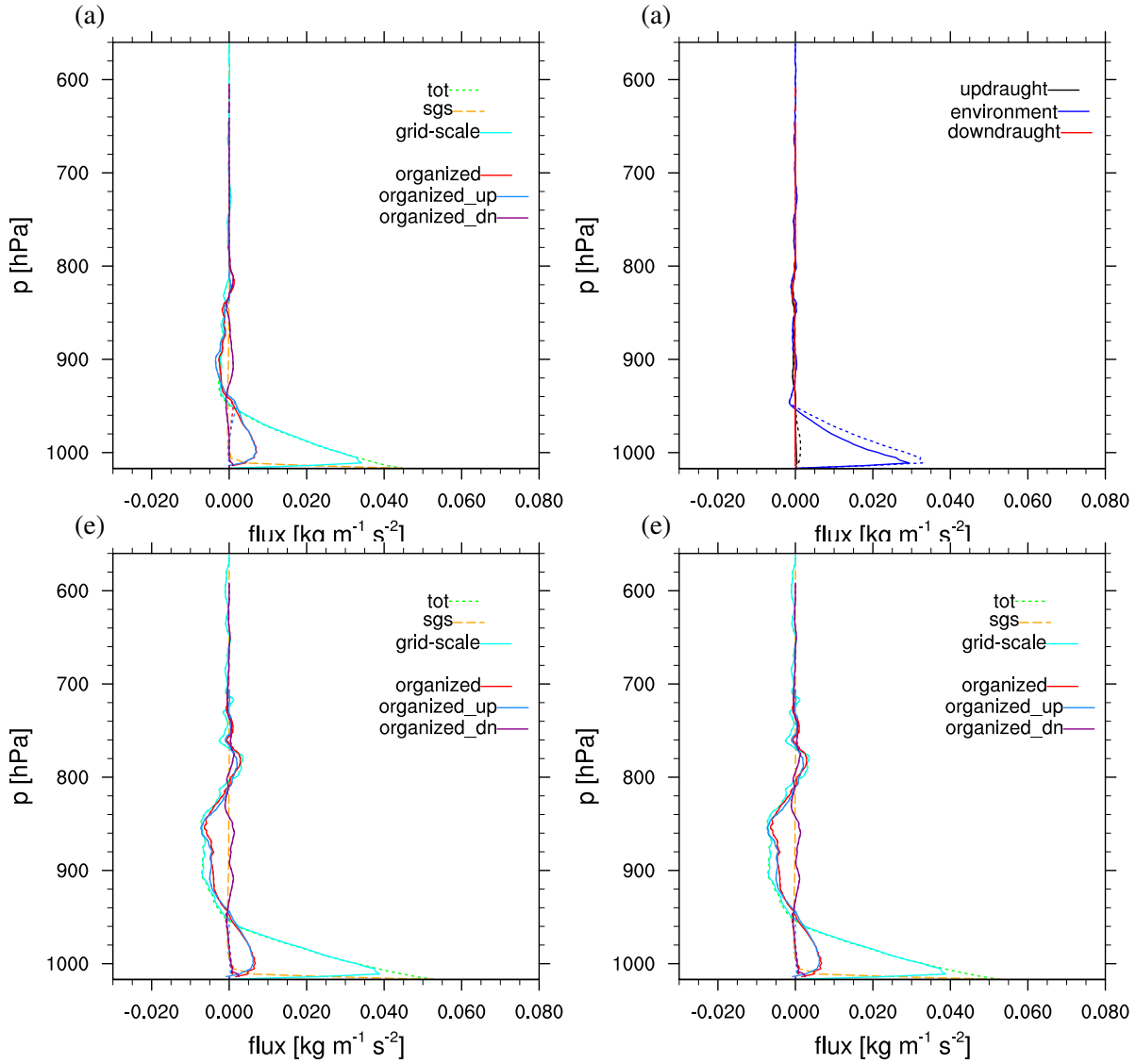


*Figure 5: Same as Fig. 3 but for the vertical flux of meridional momentum.*

denote deviations to the updraught, downdraught and environment, respectively. The first term on the RHS represents the flux caused by in-cloud fluctuations of $w$ and $\chi$, the second one in the downdraught and the third one in the environment. The fourth term on the RHS represents the organised mass-flux term. Merely this last term is considered in the mass-flux approximation, whereas the other terms are neglected:

$$\overline{w'\chi'}_{MF} \approx \sigma_u(\overline{w}^u - \overline{w})(\overline{\chi}^u - \overline{\chi}) + \sigma_d(\overline{w}^d - \overline{w})(\overline{\chi}^d - \overline{\chi}) + (1 - \sigma_u - \sigma_d)(\overline{w}^e - \overline{w})(\overline{\chi}^e - \overline{\chi}) \tag{2}$$

in the case of $\overline{w} \sim 0$ this reduces to:

$$\overline{\rho w'\chi'}_{MF} \approx M_u(\overline{\chi}^u - \overline{\chi}) + M_d(\overline{\chi}^d - \overline{\chi}) + M_e(\overline{\chi}^e - \overline{\chi}) \approx M_u(\overline{\chi}^u - \overline{\chi}) + M_d(\overline{\chi}^d - \overline{\chi}) \tag{3}$$

with the upward convective mass flux $M_u = \rho \cdot \sigma_u \overline{w}^u$, the downward convective mass flux $M_d = \rho \cdot \sigma_u \overline{w}^d$, and the mass flux in the environment $M_e = \rho \cdot (1 - \sigma_u - \sigma_d)\overline{w}^e$.

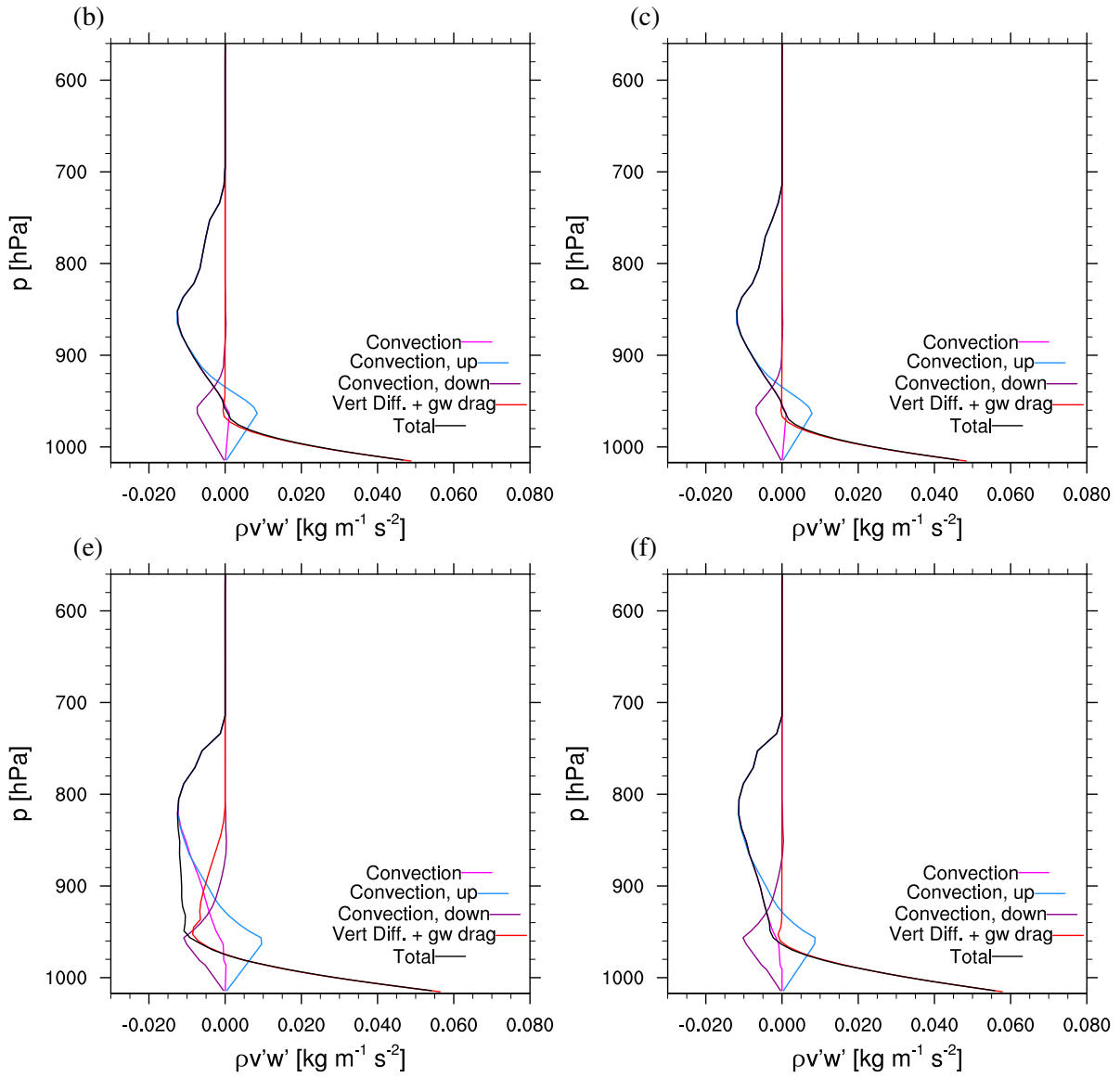


*Figure 6: Same as Fig. 4 but for the vertical flux of meridional momentum.*

The identification of up- and downdraughts in the LES data is done as follows: in the cloud layer updraughts are those grid points, where $w \geq 0.5\,\mathrm{m\,s^{-1}}$ and the cloud liquid water content exceeds $10^{-5}\,\mathrm{kg\,kg}$. Downdraughts are grid points, where $w \leq 0.5\,\mathrm{m\,s^{-1}}$. In the sub-cloud layer two different approaches are pursued to identify up- and downdraughts. In the first approach all columns directly below identified up- and downdraughts at cloud-base height are determined to be up- and downdraughts, respectively. In the second approach a height-dependent threshold for $w$ is employed. This threshold is determined such that the $\sigma_{u,cb}$ high-end part of the $w$ distribution constitutes the updraughts, where $\sigma_{u,cb}$ is the updraught fraction at cloud-base height. Likewise the $\sigma_{d,cb}$ low-end part of the distribution makes up the downdraughts. The different terms of Eq. 1 are extracted from the LES by taking the average over the entire domain ($\overline{w}$ and $\overline{\chi}$), computing the mean values over updraught, downdraught and environment areas ($\overline{w}^u$, $\overline{w}^d$, $\overline{w}^e$ $\overline{\chi}^u$, $\overline{\chi}^d$ and $\overline{\chi}^e$) and computing the deviation of $w$ and $\chi$ with respect to this mean updraught, downdraught and environment values ($w'' = w - \overline{w}^u$, $\chi'' = \chi - \overline{\chi}^u$).

Both the validity of the mass-flux approximation for CMT and an adequate representation of the organised mass-flux term determine the accuracy of the momentum-flux representation. First, we will analyse the accuracy of the mass-flux approximation, and second the representation of the organised term will be investigated. The different terms of Eq. 1 are illustrated in Fig. 3 for $\chi = u$ and in Fig. 5 for $\chi = v$ computed from the LES data. The total LES momentum flux (green line in Fig. 5 a, c) consists of a resolved flux (cyan line) and a sub-grid scale flux (dashed orange line). Due to the fine grid spacing ($\Delta x$=25 m) of the LES runs almost the entire flux is resolved by the LES and the sub-grid scale component is small, except in a thin layer close to the surface. Only the grid-scale variables from the LES are available for all further computations performed in our analysis. Ideally, the organised mass-flux term (red line) should correspond to the total grid-scale flux (cyan line). However, it covers only a part of the total vertical flux $\overline{\rho u'w'}$ and $\overline{\rho v'w'}$. For $u$ the problem is more pronounced than for $v$. A significant portion of $\overline{\rho u'w'}$ is carried by fluctuations in the environment (blue line in Fig. 3 b, d, third term on the RHS of Eq. 1), which are neglected by the mass-flux approximation. The fact that the mass-flux approximation may not capture the entire momentum flux has been discussed in Zhu (2015). Interesting to note is that the two different approaches to isolate up- and downdraughts in the sub-cloud layer in the LES data yield different results for all the quantities considered. The fluctuations within the clouds and the downdraughts (black and red line in Fig. 3 b, d) are very small, thus it is justified to neglect them in the parametrisation.

Analysis of the SCM momentum fluxes yields the following: the SCM simulated total momentum flux (black lines in Fig. 4 and 6) consists of the flux from the convection routine (magenta lines) and the flux from the vertical diffusion and gravity-wave drag (red lines). The total flux should be compared to the total flux in the LES (green line in Fig. 5 a, c). The flux from the convection routine (magenta line) is further split up into the upward flux (blue lines) and the downward flux (violet lines) and should be compared to the total, up- and downdraught parts of the organised flux in Fig. 5 a and c. It shows a rather good representation of the fluxes with height with positive values in the lower part of the atmosphere. In the upper part of the domain, however, the SCM shows negative fluxes for u, which are absent in the LES total flux, but present in the LES organised flux. While the fluxes in the sub-cloud layer fit very well, the magnitudes tends to be overestimated in the upper part of the cloud layer. In the SCM_new run the magnitude of the fluxes is overall slightly reduced as compared to the SCM run, with similar shapes of the profiles. Thus, the mass-flux limiter corrects the fluxes in the right direction. Overall, the convective flux overestimates the organised flux in the LES. This compensates partly for the fact the organised flux in the LES underestimates the total LES flux. Important to note is that the momentum flux is mostly down-gradient in the RICO case at all investigated time steps and that the upward flux of momentum is considerably stronger than the downward flux.

**Entrainment/Detrainment, mass-fluxes** Entrainment and detrainment rates represent the horizontal mass exchange between the convective plumes and the environment. They thus crucially influence the vertical profile of convective mass flux, which in turn determines the vertical transport of the required quantities. Figure 7 shows the values for mass entrainment, detrainment and convective mass flux. Fractional entrainment $\varepsilon$ and detrainment $\delta$ rates are extracted from the LES data following the bulk approach (see e.g. de Rooy et al. 2012) using:

$$\frac{\partial \phi}{\partial z} = -\varepsilon \left(\phi_c - \phi_e\right) \tag{4}$$

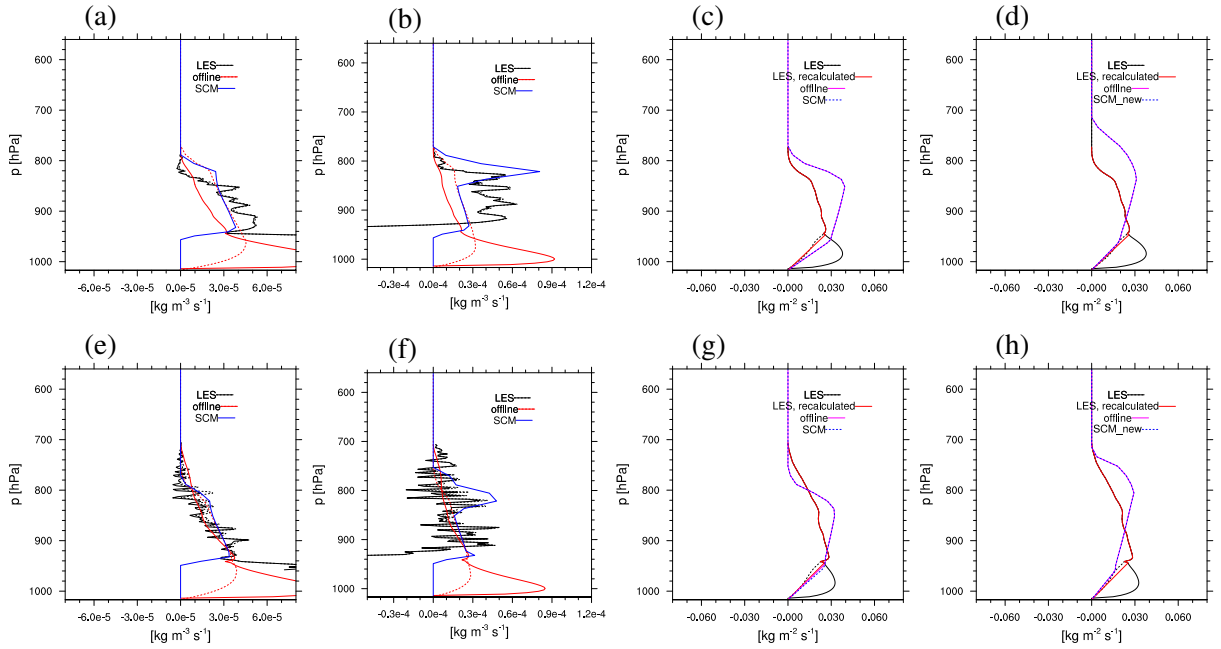


*Figure 7: (a, e) Rates of mass entrainment ($kg\,m^{-3}\,s^{-1}$) derived from the LES using $\theta_e$ as conserved variable (black solid line) or using $q_t$ as conserved variable (black dashed line), computing E from the IFS equations using LES values for convective mass flux and relative humidity (red solid line), computing entrainment from the IFS equations using SCM values for convective mass flux and relative humidity (red dashed line), as well as SCM values (blue). (b, f) Same as panel (a, e) but for D. (c, g) Upward convective mass flux ($kg\,m^{-2}\,s^{-1}$) from the LES (black solid line, in the sub-cloud layer the solid line corresponds to sampling those sub-cloud layer thermals that exceed a certain threshold, while the dashed line corresponds to sampling the areas below cloud base), recalculating mass-flux based on LES data for entrainment and detrainment (red), recalculating mass flux based on SCM values for cloud-base convective mass flux and entrainment/detrainment (magenta) and SCM values (blue). (d, h) same as (c, g) but for SCM_new. Quantities are valid at t=10 h (upper row) and t=60 h (lower row) for the RICO case.*

$$\varepsilon - \delta = \frac{1}{M_u}\frac{\partial M_u}{\partial z} \tag{5}$$

Two different moist-conserved variables are employed for $\phi$: in the first case the total water mixing ratio ($q_t$ black dashed line in Fig. 7 a, b, e, f) and in the second case equivalent potential temperature ($\theta_e$ black solid line in Fig. 7 a, b, e, f). $\phi_c$ are in-cloud values, whereas $\phi_e$ are the values in the environment. Fractional entrainment/detrainment values from the LES are converted into values for mass-entrainment $E$ by $E = M_u \cdot \varepsilon$ and into mass detrainment $D$ by $D = M_u \cdot \delta$ using the LES values for $M_u$.

$E$ and $D$ are recalculated using the IFS parametrisation routine but using the LES values for relative humidity and $M_u$ (red solid line) or using the SCM values for relative humidity and $M_u$ (red dashed line). The same approach is followed for $M_u$, where $E$ and $D$ from the LES or SCM are employed to recompute $M_u$ offline. Both the offline calculations and the SCM capture the vertical profile of $E$ and $D$ very well at both investigated times. Detrainment in the SCM shows large values in the upper part of the cloud (blue solid line in Fig. 7 b and f), where it represents organised outflow at the cloud top. As a result SCM convective mass flux shows a vertical profile that is more top-heavy than what the LES data suggests (blue/magenta lines vs. red/black lines in Fig. 7 c and g). Even more important than the vertical profile is the prediction of the cloud-base convective mass-flux, determined by the closure. Cloud-base convective

mass-flux is overestimated in the case at hand, especially at the earlier time in the unorganised cloud field. As convective mass-flux and $E$ and $D$ are so tightly coupled, the cloud-base mass-flux reflects itself also in the vertical profiles of those quantities. Thereby, the difference between the red solid and red dashed line in Fig. 7 a, b, e and f can be understood. The larger values of cloud-base mass flux and the different relative humidity in the SCM yield larger entrainment/detrainment rates (red dashed line) than using LES values (red solid line). The revised formulation for the convective mass flux in SCM_new yields smaller values of cloud-base convective mass flux, which is even smaller than the LES values. The mass-flux profile is deeper in SCM_new than in SCM, leading to an overall better representation of $M_u$. Yet, the profile is still top-heavy, while the LES suggests a bottom-heavy profile.

**Momentum in up- and downdraughts** For the computation of the momentum flux, the in-cloud values for the momentum $u_u$ and $v_u$ are required. There are several challenges connected with their prediction. First, the horizontal winds are affected by the horizontal pressure gradient across the updraught, which accelerates the in-cloud winds (see e.g. Kershaw and Gregory 1997). The importance of the pressure-gradient term has been investigated for deep convection (e.g. Grubišić and Moncrieff 2000), but little is known about its importance for shallow convection. Second, values for the horizontal momentum at cloud base are unknown. In the IFS, the value at cloud base $u_{u,cb}$ is set to the environmental value at the departure level for convection. The in-cloud values for $u$ are then predicted going upward from cloud base:

$$\frac{\partial M_u \bar{u}_u}{\partial z} = E_u \bar{u} - D_u \bar{u}_u - \underbrace{\overline{\sigma_u \left(\frac{\partial p}{\partial x}\right)_u}}_{\text{pressure-gradient term}} \tag{6}$$

Below cloud base, a linear decrease of the momentum flux with height is assumed. The pressure-gradient term is currently neglected in the IFS in the prediction of $u_u$. Finally, a correction term is applied to the updraught velocities:

$$u_u = u_u - u_{pert}\,\text{sign}(u_u) \quad \text{and} \quad v_u = v_u - u_{pert}\,\text{sign}(v_u) \tag{7}$$

with $u_{pert}$= 0.3 m s$^{-1}$. As will be shown later this function exhibits a discontinuity at $u_u = 0$ m s$^{-1}$. Thus, we propose here to replace the formulation for the correction term by:

$$u_u = u_u - min(|u_u|, u_{pert})\,\text{sign}(u_u) \quad \text{and} \quad v_u = v_u - min(|v_u|, u_{pert})\,\text{sign}(v_u) \tag{8}$$

This new formulation for the correction term is used in Figure 8 (red and orange dashed line).

The pressure-gradient term is extracted from the LES by first calculating the local pressure gradient $\frac{\partial p}{\partial x}$ and $\frac{\partial p}{\partial y}$, respectively, by a forward difference. Then, these values are averaged over the updraught areas as described above. As the local derivatives $\frac{\partial p}{\partial x}$ and $\frac{\partial p}{\partial y}$ average out in the interior of the updraught the resulting values reflect the pressure gradient across the entire updraught.

In the LES data the in-cloud momentum is smaller than the domain-mean value in the lower part of the clouds but becomes larger than the domain-mean value in the upper part of the clouds (black line in Fig. 8). In order to test the validity of the employed parametrisation the values are step by step recalculated offline. To this end Eq. 6 is integrated inserting directly LES-derived data for $u_{u,cb}$, $\bar{u}$, $M_u$, $E_u$ and $D_u$. The red lines in Fig. 8 display these recalculated values with (dashed red line) and without (solid red line) the correction term (Eq. 8). Ideally, the red solid lines should match the black line. The first apparent issue is the mismatch of the cloud-base value for $u_u$. The value is too small for $u$ but too large for $v$.

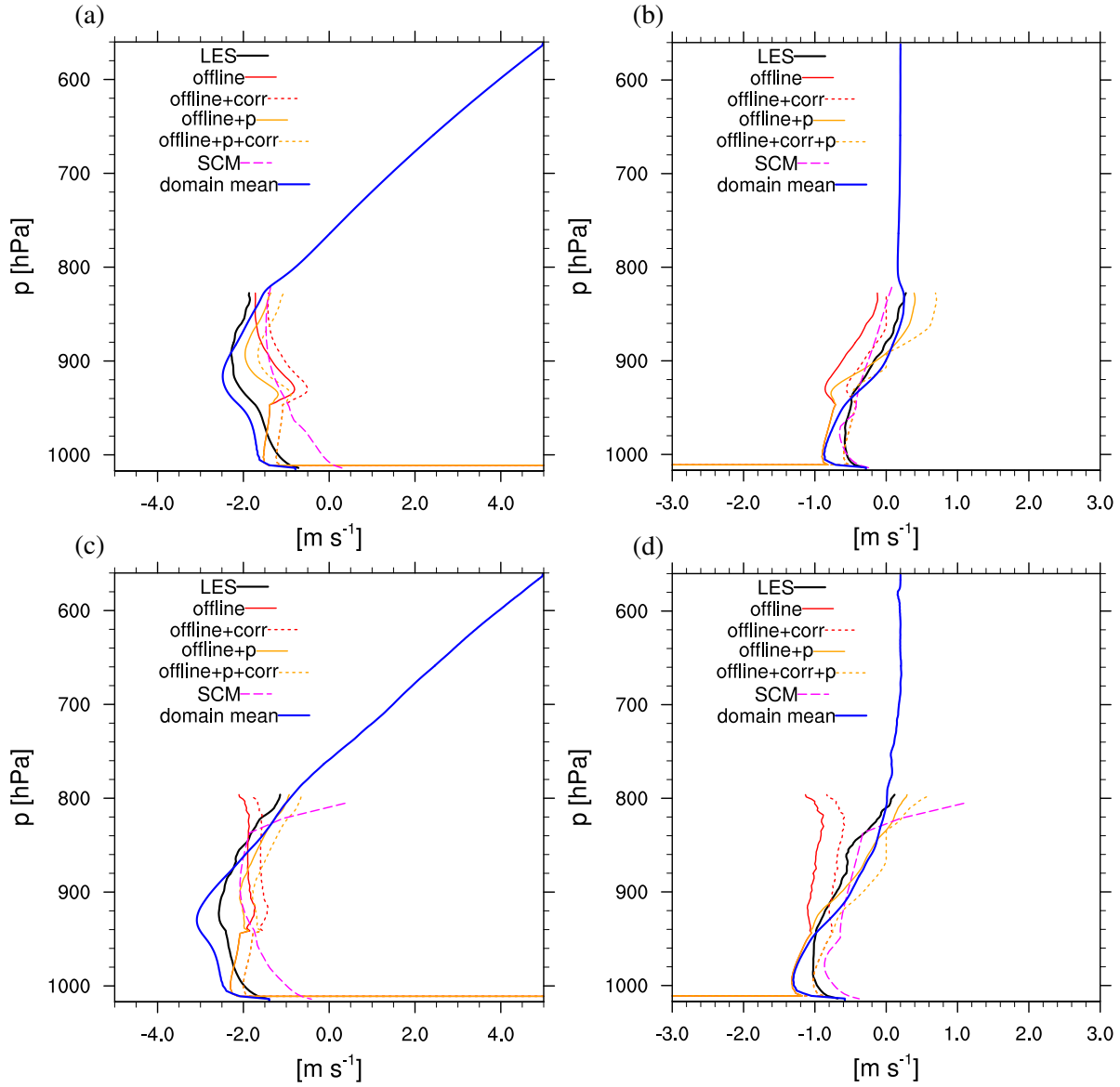


*Figure 8: In-cloud momentum as extracted from the LES (black solid), recalculated using LES values following the IFS routines (red), recalculated using LES values following the IFS routines and adding the pressure-gradient term (orange), values from the SCM (magenta) and domain-mean values in the LES (blue). The effect of applying the perturbation to the in-cloud values is illustrated by the dashed red and orange lines. (a) and (c) display values for u, whereas (b) and (d) show v; the upper row is valid at 10 h and the lower row at 60 h.*

The correction term thus yields a good correction for $v$, whereas it deteriorates $u$. The influence of the pressure-gradient term onto $u_u$ is illustrated by the orange lines, for which the LES-derived pressure-gradient term has been added for the in-cloud momentum (cf. Eq. 6). While the effect of the pressure gradient is small near cloud base, it increases towards the cloud top, yielding a better-matching profile with height. The impact of $M_u$, $E_u$, $D_u$ are finally assessed in the magenta line, where $u_u$ is extracted directly from the SCM. For $u$ the SCM values are considerably smaller than the LES values, which stems from a different value of $u_{u,cb}$. The vertical profile differs from the offline-calculated values due to the different values for $u_{u,cb}$, $v_{u,cb}$, $M_u$, $E_u$, $D_u$. A general finding from the analysis is, that retrieving cloud-base values for both convective mass-flux and in-cloud momentum is crucial, but difficult. The shape of the vertical profiles on the other hand are relatively well-predicted by the IFS routine.

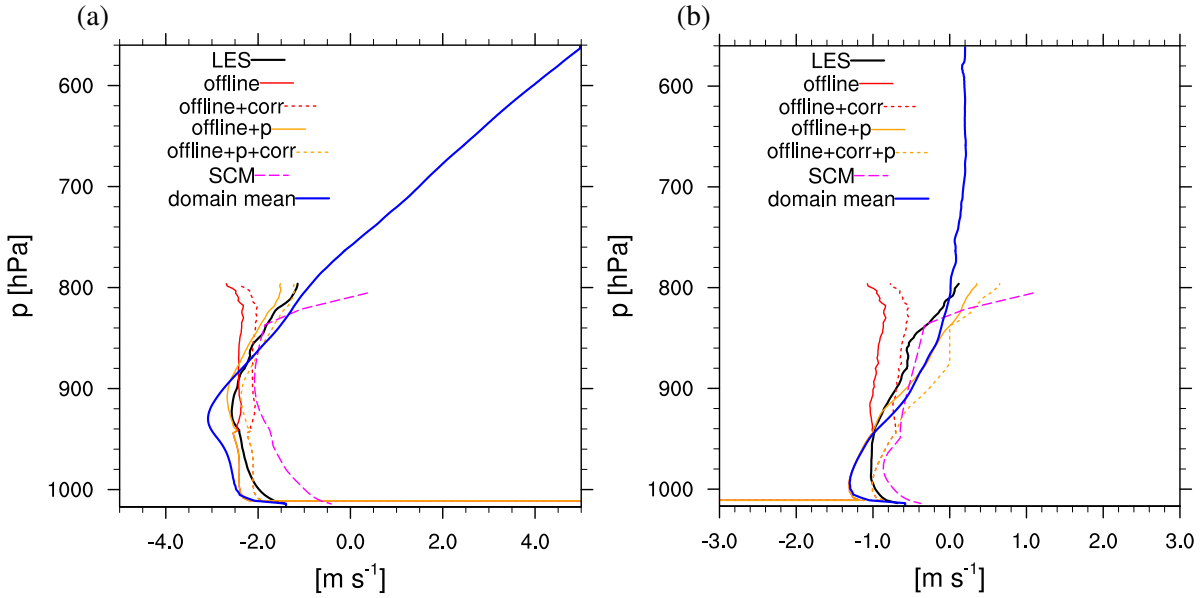


*Figure 10: In-cloud momentum as extracted from the LES (black solid), recalculated using LES values following the IFS routines (red), recalculated using LES values following the IFS routines and adding the pressure-gradient term (orange), values from the SCM (magenta) and domain-mean values in the LES (blue). The effect of applying the new perturbation (cf. Eq. 9) to the in-cloud values is illustrated by the dashed red and orange lines. (a) displays values for u, whereas (b) shows v; the data is valid at 60 h.*

As mentioned earlier Eq. 7 is discontinuous at $v_u = 0\,\mathrm{m\,s^{-1}}$. This is illustrated in Fig. 9, where $v_u$ jumps from a value of $u_{pert}$ to $-u_{pert}$ (blue line). Using Eq. 8 (dashed orange line) $v_u$ remains at a value of $0\,\mathrm{m\,s^{-1}}$ in the interval $v_u \in [-0.3, 0.3]\,\mathrm{m\,s^{-1}}$.

We investigate a further modification to the in-cloud values for momentum. Instead of setting $u_{u,cb}$ and $v_{u,cb}$ to the value of $\bar{u}$ and $\bar{v}$ at the departure level, we take the average value between the departure level and the value at cloud base:

$$u'_{u,cb} = \frac{\bar{u}_{idpl} + \bar{u}_{cb}}{2} \tag{9}$$

This indeed matches the values at cloud base better, as visible in Fig. 10. Using the formulation of Eq. 9 the correction term should however be abandoned. As a result, the entire profile of the offline recalculated values of $u_u$ and $v_u$ match the LES results better (orange dashed line vs black line). In the determination of $u_{u,cb}$ and $v_{u,cb}$ from the LES data one should keep in mind that the profiles of $\bar{u}$ and $\bar{v}$ exhibit a strong bend in the surface layer due to friction, which may not be as pronounced in the IFS. Thus, values at the departure level may well differ between the LES and IFS, which in turn affects

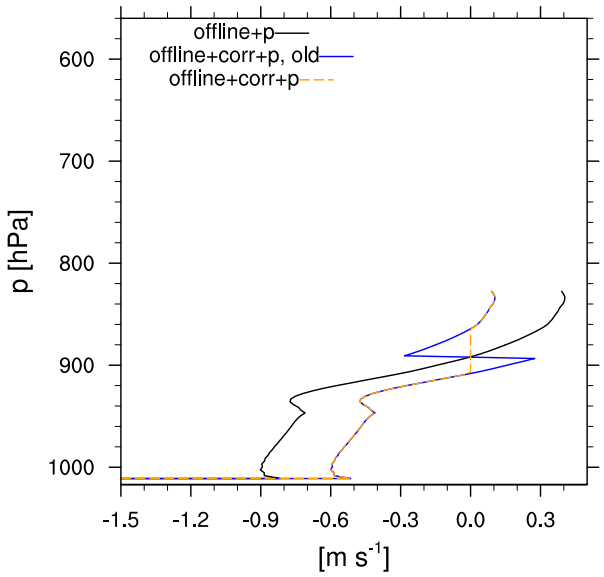


*Figure 9: $v_u$ at 10 h recalculated using LES values following the IFS routines and adding the pressure-gradient term (black), applying the correction term following Eq. 7 (blue) and applying the correction term following Eq. 8 (orange dashed).*

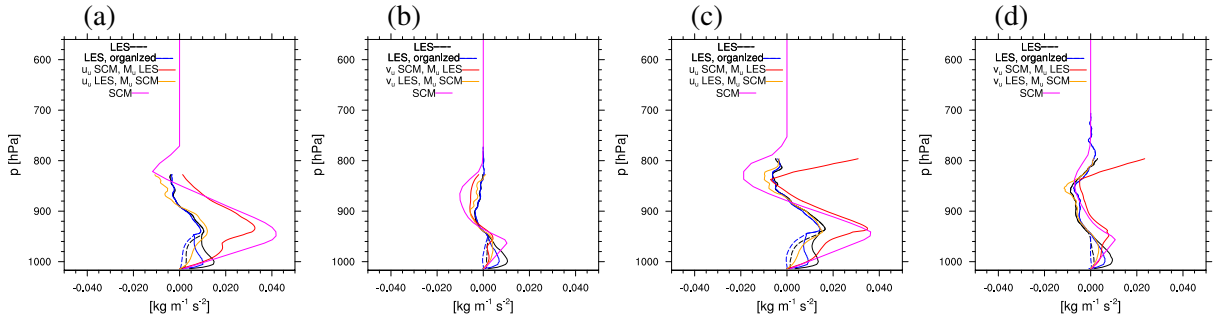


*Figure 11: Upward momentum flux (kg $m^{-1}$ $s^{-2}$) as extracted from the LES (black solid), the organised mass-flux term from the LES (blue solid), recalculated using SCM values for $u_u$ but $M_u$ from the LES (red), recalculated using LES values for $u_u$ but $M_u$ from the SCM and values from the SCM (magenta). (a) and (c) display values for u, whereas (b) and (d) show v; the upper row is valid at 10 h and the lower row at 60 h.*

$u_{u,cb}$ and $v_{u,cb}$.

Taking the terms $M_u$, $u_u$ and $\overline{u}$ together to finally retrieve the desired updraught convective momentum flux $\rho\overline{u'w'} \approx M_u(u_u - \overline{u})$ (cf. Eq. 3) yields the following picture: the mass-flux approximation captures most of the vertical momentum transport in the updraughts (comparing the blue with the black lines in Fig. 11). Fig. 11 further suggests that an appropriate representation of the in-cloud values of momentum is more critical than the representation of convective mass flux. Using the mass flux from the SCM but the in-cloud values from the LES (orange line) yields a better result than using the in-cloud values from the SCM in combination with the convective mass flux from the LES (red line). However, the convective mass flux and the entrainment/detrainment rates also enter the prediction of the vertical profiles of in-cloud values (cf. Eq. 6). Thus, it is difficult to separate these two players entirely.

**Pressure-gradient term** As outlined above the pressure gradient across updraughts affects the in-cloud values for momentum. Different ways to parametrise this effect have been proposed. Both the importance of the pressure-gradient term and the different parametrisation approaches are assessed in the following. Averaging the horizontal momentum equation and assuming steady-state conditions gives (cf. Eq. 6):

$$\frac{\partial}{\partial z}\left(\rho\sigma_u\overline{u'w'}_u\right) = E\overline{u} - D\overline{u}_u - \sigma_u\overline{\left(\frac{\partial p}{\partial x}\right)}_u \tag{10}$$

Applying the mass-flux approximation and using Eq. 5 results in:

$$M_u\frac{\partial\overline{u}_u}{\partial z} = E\left(\overline{u} - \overline{u}_u\right) - \sigma_u\overline{\left(\frac{\partial p}{\partial x}\right)}_u \tag{11}$$

Hence, the divergence of the vertical momentum flux is balanced by entrainment and detrainment across the updraught, plus the action of the pressure-gradient force. The role of the pressure gradient in this balance is quantified by investigating the residual between the flux-divergence and the first two terms on the right-hand side of Equation 10:

$$\mathscr{R}_1 = \frac{\partial}{\partial z}\left(\rho\sigma_u\overline{u'w'}_u\right) - E\overline{u} - D\overline{u}_u \tag{12}$$

and the residual in Equation 11:

$$\mathscr{R}_2 = M_u\frac{\partial\overline{u}_u}{\partial z} - E\left(\overline{v} - \overline{v}_u\right) \tag{13}$$

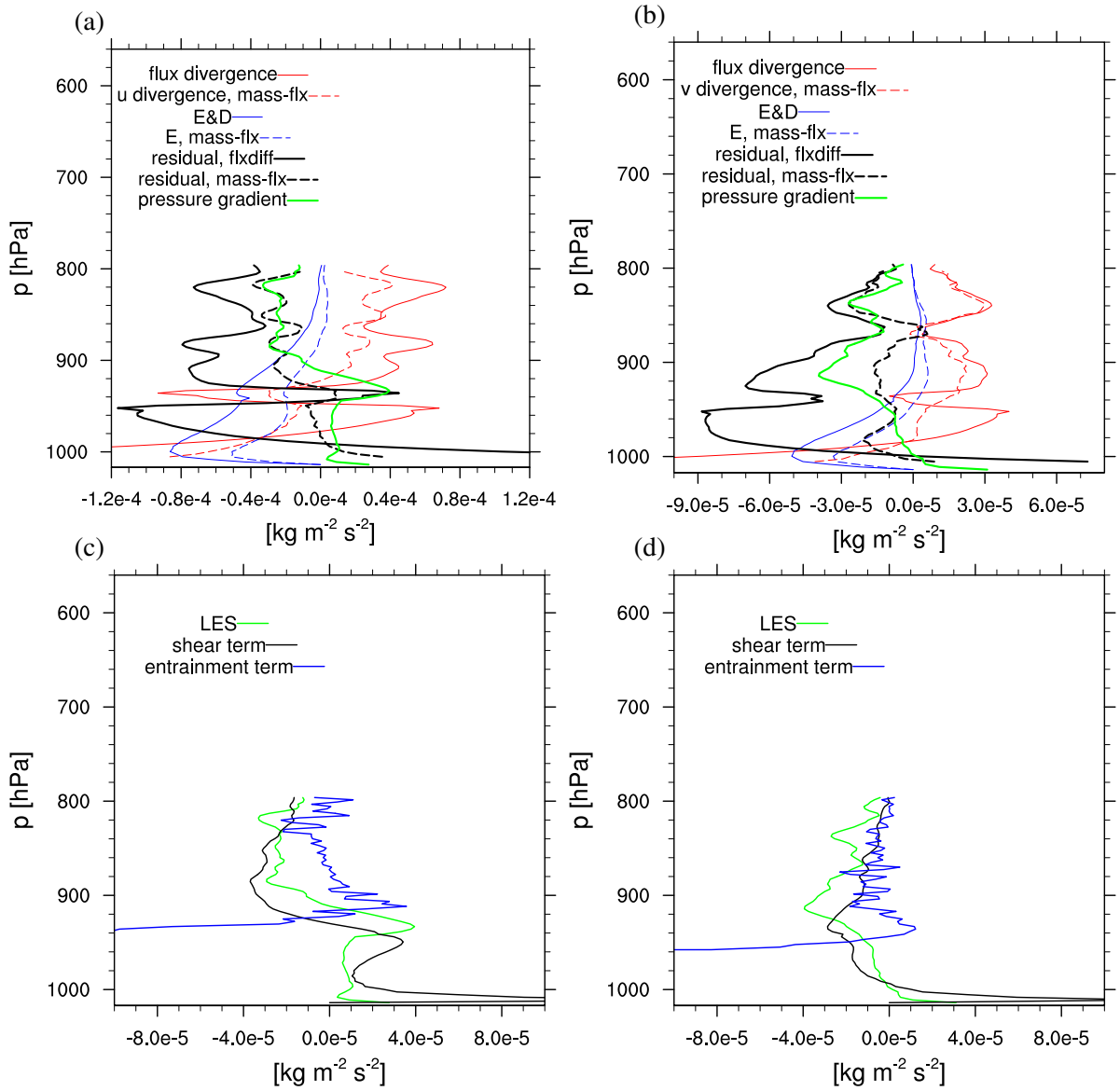


*Figure 12: Upper row: Flux divergence (red) and entrainment/detrainment term (blue) using Eq. 10 (solid lines) and applying the mass flux approximation (Eq. 11, dashed lines), $\mathscr{R}_1$ (solid black), $\mathscr{R}_2$ (dashed black line) and pressure-gradient term (green) for (a) u and (b) v. Lower row: Different approaches for parametrising the pressure-gradient term (green) using vertical wind shear (black) or a modified detrainment rate (blue) for (c) u and (d) v. All graphs are valid at 60 h. The red lines in panel a and b have been smoothed by applying a 6-point running average to the data.*

Figure 12 illustrates the individual terms of Equation 10 and 11. Within the mass-flux approximation the pressure-gradient term (green line) matches the residual $\mathscr{R}_2$ (black dashed line) approximately. However, its magnitude is considerable, exceeding the entrainment term especially in the upper part of the cloud. This non-negligible influence on the in-cloud values of momentum in the upper part of the cloud was also apparent in Fig. 6. The residual $\mathscr{R}_1$ (black solid line) is larger than $\mathscr{R}_2$ and exceeds the pressure-gradient term. This is also true for the other terms of Eq. 10, where each individual term is larger than under the mass-flux approximation. Hence, the pressure-gradient term can explain the missing in-cloud momentum not captured by entrainment/detrainment within the mass-flux framework. However, in order to represent the entire divergence of in-cloud momentum-flux, the pressure-gradient term cannot make

up for the whole part missed by the entraining/detraining plumes but there are additional missing parts. The difference between $\mathscr{R}_1$ and $\mathscr{R}_2$ is of about equal magnitude as $\mathscr{R}_2$ itself. One possible interpretation is that the errors introduced by applying the mass-flux approximation are of the same order of magnitude as neglecting the pressure-gradient term.

Different practices for parametrising the pressure-gradient term have been suggested. While Kershaw and Gregory (1997) or Gregory et al. (1997) emphasise the role of the vertical advection of momentum and parametrise it based on wind shear as

$$\sigma_u \overline{\left(\frac{\partial p}{\partial x}\right)}_u = -C_1 M_u \frac{\partial u}{\partial z} \tag{14}$$

Tiedtke (1989) focusses on the horizontal advection of momentum and thus increases the detrainment rate:

$$\sigma_u \overline{\left(\frac{\partial p}{\partial x}\right)}_u = -C_2 D_u \left(\overline{u} - \overline{u}_u\right) \tag{15}$$

(see also Brown 1999; Grubišić and Moncrieff 2000). The effect of these two different approaches is illustrated in Fig. 12 c and d using the values $C_1 = 0.7$ and $C_2 = 2$. While the green line shows the LES data, the blue and black lines illustrate the two different parametrisations. Both approaches capture the vertical shape of the profile from the LES and show a good behaviour in the middle of the cloud. Around cloud base, they both show limitations. Thus, both Eq. 14 and 15 are appropriate to account for the pressure-gradient term in the calculation of in-cloud momentum.

**Downdraught** In addition to the momentum flux carried by the updraughts downdraughts contribute to the total momentum flux (cf. Fig. 3 and 5), albeit less. Thus, we compare the LES-derived downdraught mass-flux $M_d$ with the SCM values, as well as the momentum values inside the downdraughts $u_d$ and $v_d$. The mass-flux inside the downdraughts is considerably larger in the LES than the values predicted by the SCM (Fig. 13 a and d). In addition, the vertical profile differs. While the SCM determines a maximum value around cloud-base height, the LES data suggest a maximum in the middle of the cloud layer. This could be related to the driving mechanism for the downdraughts for the shallow clouds. While in deep convection downdraughts are primarily driven by the evaporation of precipitation and melting of hydrometeors, evaporation of cloud droplets could play a more important role in shallow convection. Analysis of the values of momentum in the downdraughts shows that it differs surprisingly little from the domain mean values (Fig. 13 b, c, e, f). This is in contrast to the findings of Kershaw and Gregory (1997) who found values of the downdraught momentum to resemble updraught values. They thus concluded that downdraughts are mainly composed of air which has previously ascended in an updraught. One possible explanation for the small difference in the RICO case could be that the analysed shallow convection exhibits few coherent downdraughts and that our sampling strategy identifies disorganised structures, where momentum is carried downward over short distances. For highly turbulent downdraughts one can further imagine an efficient exchange of momentum between the downdraught and the environment.

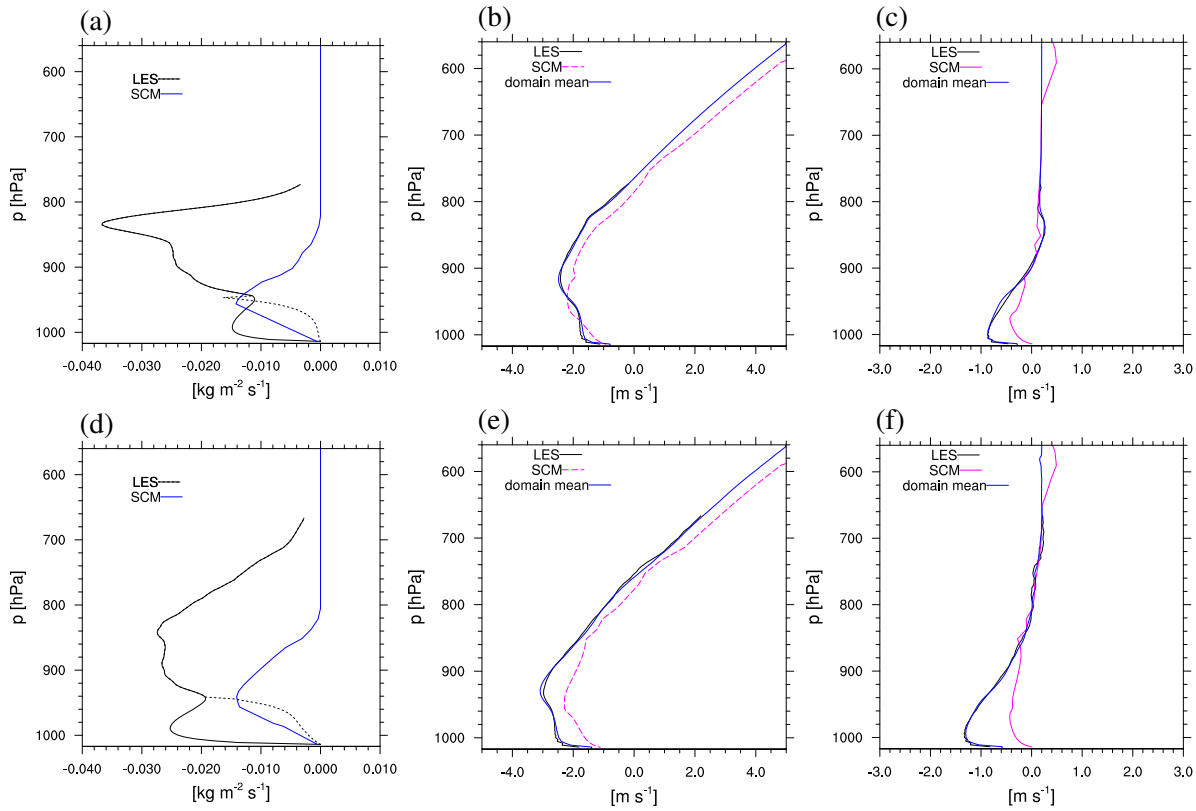


*Figure 13: (a, d) Downdraught convective mass flux (kg $m^{-2}$ $s^{-1}$) from the LES (black solid line, in the sub-cloud layer the solid line corresponds to sampling those sub-cloud layer thermals that exceed a certain threshold, while the dashed line corresponds to sampling the areas below downdraughts at cloud base) and SCM values (blue). (b, e) $u_d$ inside the downdraught and (c, f) $v_d$ inside the downdraught as extracted from the LES (black solid), values from the SCM (magenta) and domain-mean values in the LES (blue). Quantities are valid at t=10 h (upper row) and t=60 h (lower row) for the RICO case.*

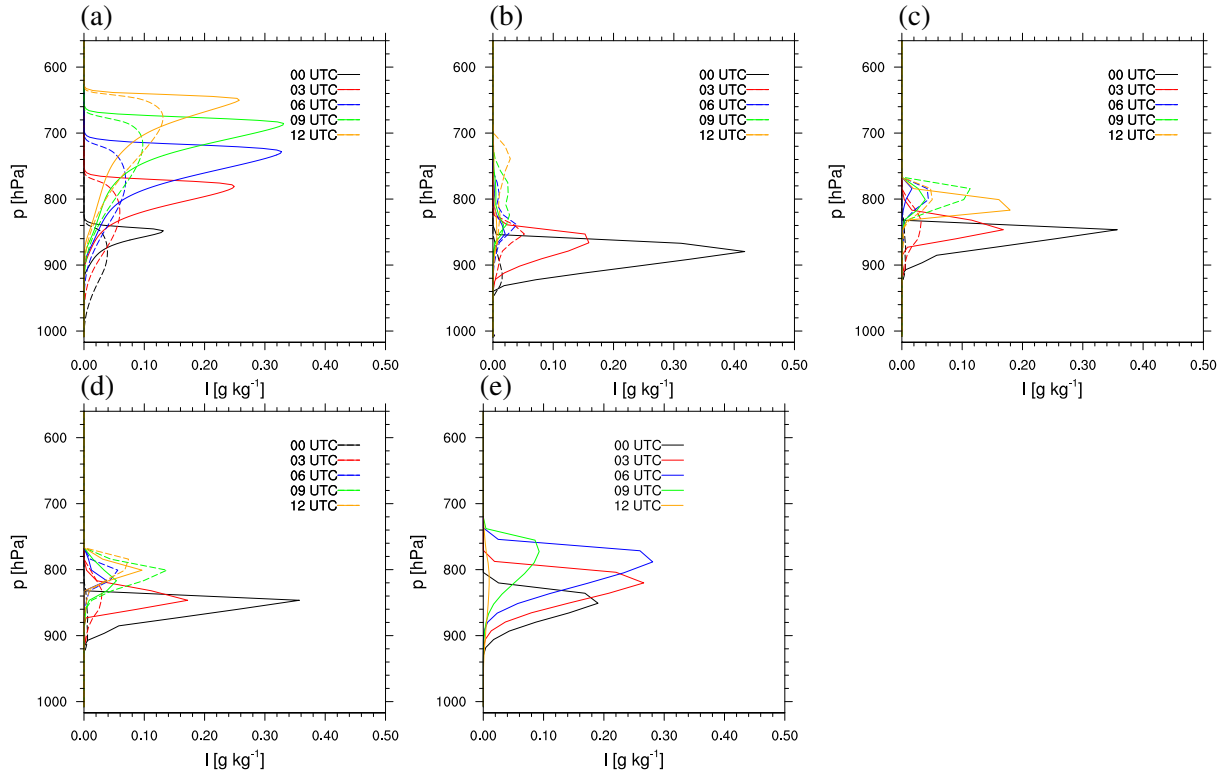


*Figure 14: Specific liquid water content ($g\,kg^{-1}$, solid lines) and specific cloud ice water content ($g\,kg^{-1}$, dashed lines) on January 31st, 2010 in (a) the LES, (b) the IFS , (c) the SCM simulations, (d) the SCM_new simulation and (e) in the UM LAM.*

## 3.2 CONSTRAIN

### *3.2.1 Overview*

In the CONSTRAIN case mixed-phase clouds develop at the top of the mixed-layer (Fig. 14). As the air is advected southward over warmer SST the mixed layer deepens and the clouds shift upward. Both liquid water and ice water content is larger in the LES than in the IFS simulation and the mixed-layer is deeper. Moreover, the clouds dissolve earlier in the IFS and the fraction of ice clouds is smaller. However, the IFS produces a larger cloud fraction (not shown). The SCM simulates a state that is similar to the one in the IFS with a somewhat deeper mixed layer. Clouds moreover take longer to dissolve. In SCM_new liquid and ice water content are slightly smaller and situated at a lower altitude in comparison to SCM. The Met Office Unified Model (UM) limited area model (LAM) simulations that were used to design the CONSTRAIN case show a comparable magnitude of the liquid water content as the LES but an overall shallower boundary layer.

The meridional wind shows a strong increase with height (Fig. 15). In particular, there is a distinct jump across the inversion. This jump is visible both in the LES and IFS, whereas it is more pronounced for the zonal wind in the LES than in the IFS. In accordance with the deeper mixed layer it is situated further up in the LES. The SCM simulates a state close to the LES and IFS for the early times of the simulation (00 UTC and 03 UTC), but the momentum differs considerably at the later times.

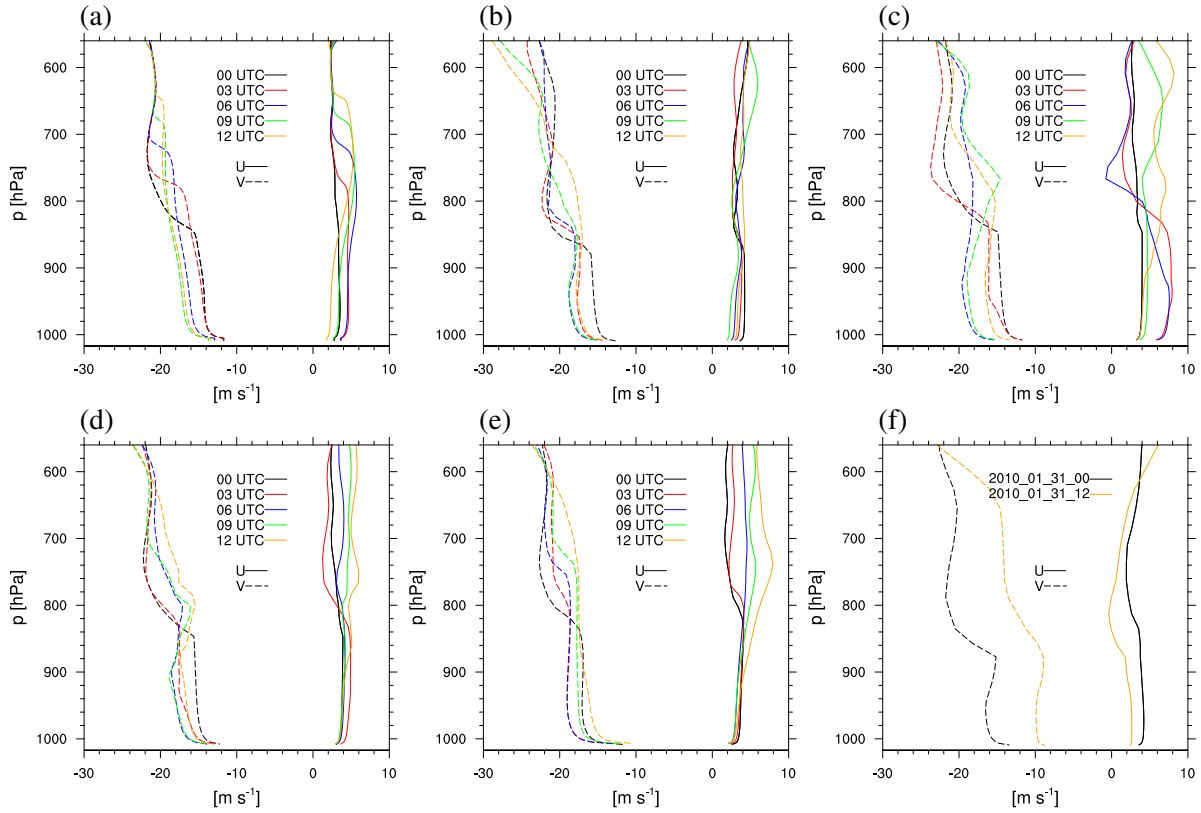


*Figure 15: Zonal (solid) and meridional (dashed) wind ($m\,s^{-1}$) on January 31st, 2010 in (a) the LES, (b) the IFS, (c) the SCM simulations, (d) the SCM_new simulation, (e) in the UM LAM and (f) the ECMWF analysis.*

As done for the RICO case above, the momentum fluxes and their underlying parametrisation will be scrutinised in the following. The focus will be on 31 January 2010, 03 UTC, when a well-mixed layer has developed and the cloud layer is still well-defined both in the LES and IFS simulations. This time of analysis is 4.5 h into the LES simulation and 18 h into the IFS run. Since mixed phase clouds are analysed the criterion for the updraught selection is adapted: in the cloud-layer updraughts are those grid points, where $w \geq 0.5\,\mathrm{m\,s^{-1}}$ and the cloud liquid water content or the ice water content exceeds $10^{-5}$ kg kg.

### 3.2.2 *Analysis of the parametrised terms*

**Momentum fluxes** As in the RICO case momentum fluxes are down-gradient (Fig. 16) with a negative flux of zonal momentum and a positive flux of meridional momentum up to the inversion. Some flux occurs across the inversion for $u$ which is absent for $v$. In the LES data a larger fraction of the total flux is sub-grid scale than in the RICO LES data. This is due to the coarser grid-spacing of $\Delta$x=250 m employed. The organised mass-flux term (cf. Eq. 1) captures only a part of the total momentum flux, as significant variations occur in the environment, inside the clouds and within the downdraughts (red vs. cyan line in Fig. 16 a and c). The organised flux of zonal momentum (Fig. 16 a) even shows positive fluxes between 900 and 950 hPa, while the total flux is negative in this region. The fluxes within the clouds, the downdraughts and the environment are considerable (Fig. 16 b and d). The IFS and SCM (Fig. 17) overestimate the momentum fluxes and show a maximum at cloud-base height, while the vertical profile in the LES shows a different structure for $u$ and $v$ and emphasises the fluxes inside the cloud layer. The positive flux of $u$ across the inversion is reproduced in the SCM runs, while it is missing in the

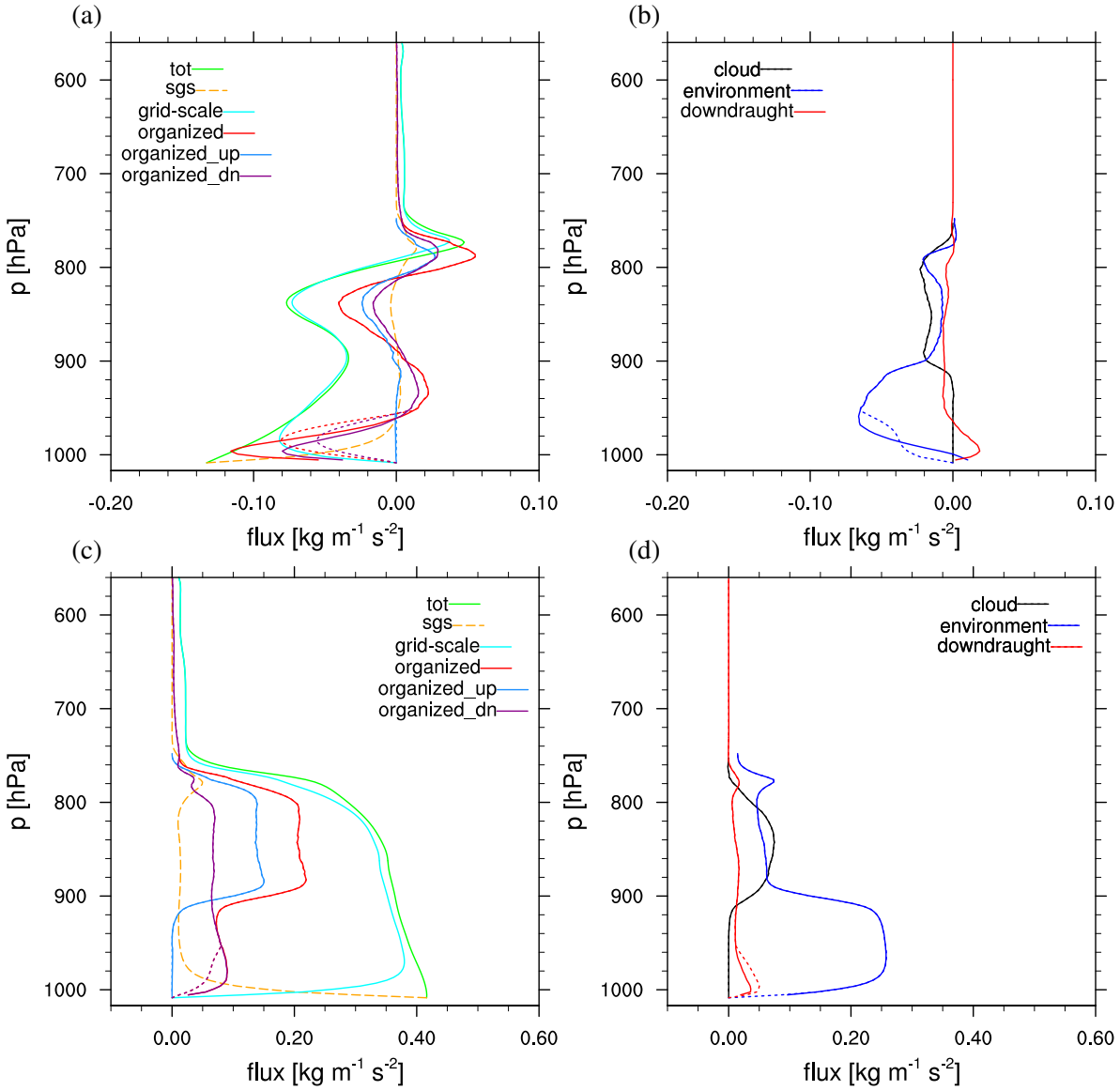


*Figure 16: Total (green), sub-grid scale (orange dashed line) and grid-scale (cyan) vertical flux of (a) zonal and (c) meridional momentum (kg $m^{-1}$ $s^{-2}$) in the LES. The total organised vertical flux of zonal momentum (kg $m^{-1}$ $s^{-2}$, cf. Eq. 1) as recomputed from the LES data (red) is further split up into the updraught (blue) and downdraught (violet) contribution. Panels (b) and (d) show the updraught (black), environment (blue) and downdraught (red) components (cf. Eq. 1) of the vertical flux as recomputed from the LES for (b) zonal and (d) meridional momentum. All graphs are valid at 31 January 2010, 03 UTC.*

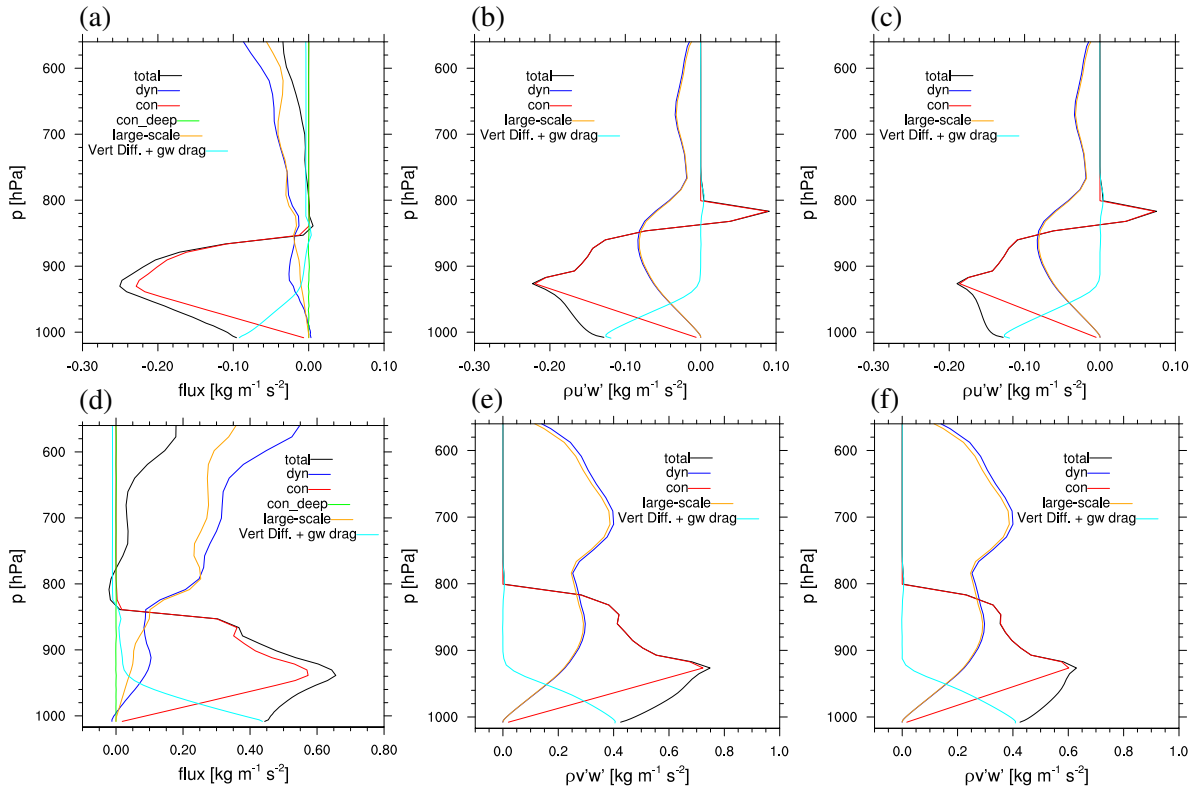


*Figure 17: Different contributions to the momentum flux ($kg\,m^{-1}\,s^{-2}$) at 31 January 2010, 03 UTC in the (a, d) IFS, (b, e) SCM and (c, f) SCM_new. The upper row shows the vertical flux of zonal momentum and the lower row the vertical flux of meridional momentum.*

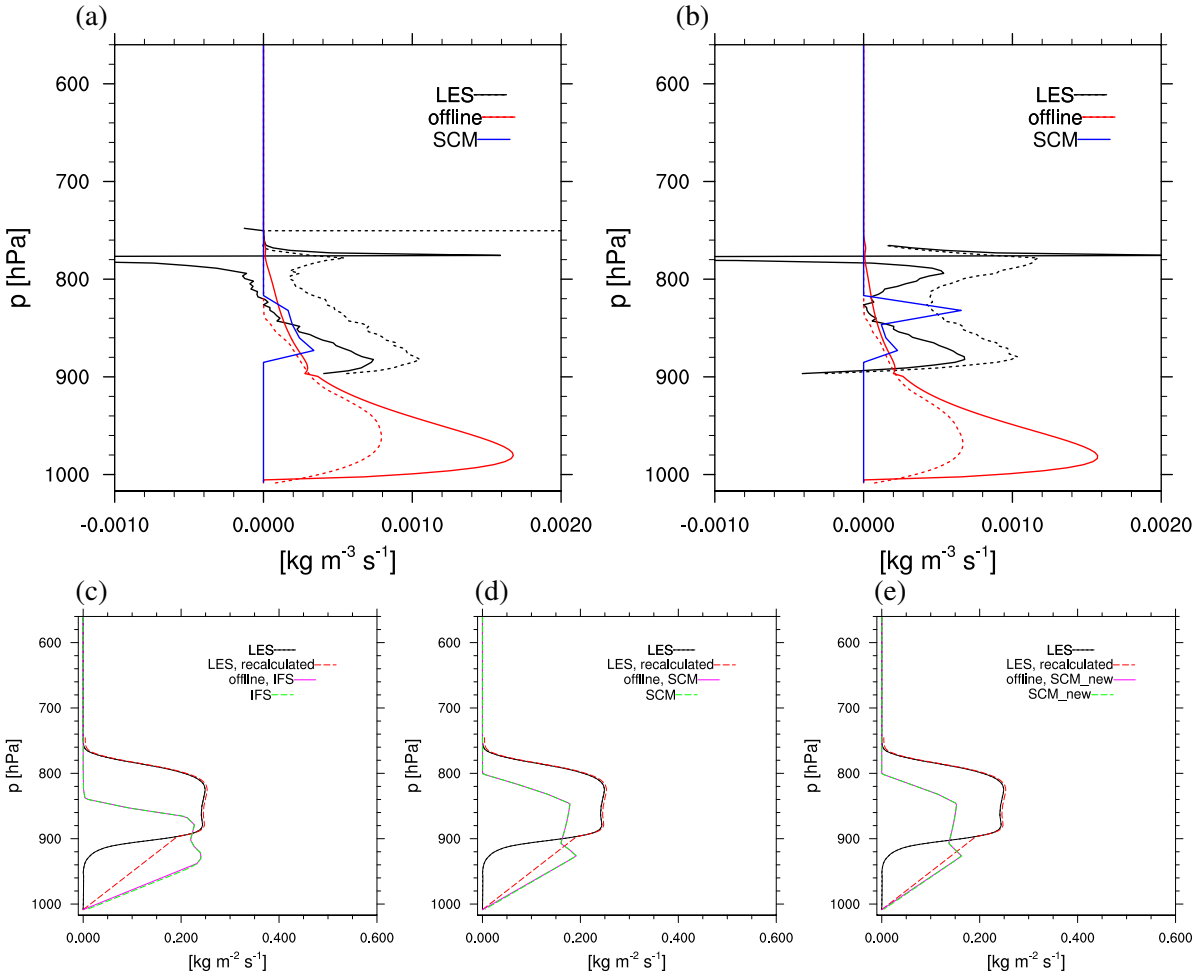


*Figure 18: (a) Rates of mass entrainment E ($kg\,m^{-3}\,s^{-1}$) derived from the LES using $\theta_e$ as conserved variable (black solid line) or using $q_t$ as conserved variable (black dashed line), computing E from the IFS equations using LES values for convective mass flux and relative humidity (red solid line), computing entrainment from the IFS equations using IFS values for convective mass flux and relative humidity (red dashed line), as well as SCM values (blue). (b) Same as panel (a) but for D. (c, d, e) Upward convective mass flux ($kg\,m^{-2}\,s^{-1}$) from the LES (black solid line, in the sub-cloud layer the solid line corresponds to sampling those sub-cloud layer thermals that exceed a certain threshold, while the dashed line corresponds to sampling the areas below cloud base), recalculating mass-flux based on LES data for entrainment and detrainment (red), recalculating mass flux based on IFS/SCM values for cloud-base convective mass flux and entrainment/detrainment (magenta) as well as data from the IFS/SCM run (green dashed line). IFS simulations are shown in panel (c) while SCM results in panel (d) and SCM_new results in panel (e). Quantities are valid at 31 January 2010, 03 UTC.*

IFS. SCM_new reduces the momentum flux as compared to SCM and shows thus a slightly improved representation.

**Entrainment/Detrainment, mass-fluxes** Figure 18 illustrates $E$, $D$ and $M_u$ as extracted from the LES, results from offline calculations using LES data for relative humidity and $M_u$ but following the IFS routines and SCM data. Unfortunately, there is no data for $E$ and $D$ available directly from the IFS. LES-derived entrainment and detrainment values are larger than offline computed values and SCM values both for entrainment and detrainment. There is however some discrepancy between the values derived based on $q_t$ and those derived using $\theta_e$ (black dashed vs black solid line in Fig. 18 a and b). As already

visible for the RICO case $D$ shows a minimum in the middle part of the cloud and a peak at cloud top, representing the organised detrainment. This peak is less pronounced in the LES data, with a stronger occurrence using $q_t$ for the calculations than using $\theta_e$. Convective mass flux is of comparable magnitude in the LES and IFS simulation, but lies at a lower altitude in the IFS. SCM values for $M_u$ are comparable to the IFS, with the cloud base at roughly the same height, but deeper clouds. $M_u$ is reduced in SCM_new due to the employed mass-flux limiter. As seen for the RICO case, predicting cloud-base convective mass flux appropriately is crucial for a correct representation of the entire profile.

**Momentum in up- and downdraughts** The in-cloud momentum $u_u$ and $v_u$ for the LES and IFS simulation are documented in Fig. 19. Using the momentum at the departure level for convection as a proxy for the cloud-base values leads to an underestimation of both $u_{u,cb}$ and $v_{u,cb}$. Thus, the perturbation $u_{\text{pert}}$ (cf. q. 8) deteriorates $u_u$ and $v_u$. Overall the pressure gradient has relatively little influence and tends to pull the profile into right direction in the upper part of the cloud layer.

Using the mean value between $u_u$ at the departure level and $u_{cb}$ (see Eq. 9) is illustrated in panels (c) and (d). It shows an overall improvement for $u_u$ and $v_u$. As suggested for the RICO case, the correction term then becomes obsolete.

Finally, looking at the momentum flux in Figure 20 significant differences are visible between the different realisations. Both differences in the in-cloud momentum and the convective mass flux between the LES and IFS data result in profiles with different shapes that are located at different altitudes. From the current analysis it is not clear if it is more important to predict the mass flux or the in-cloud momentum correctly.

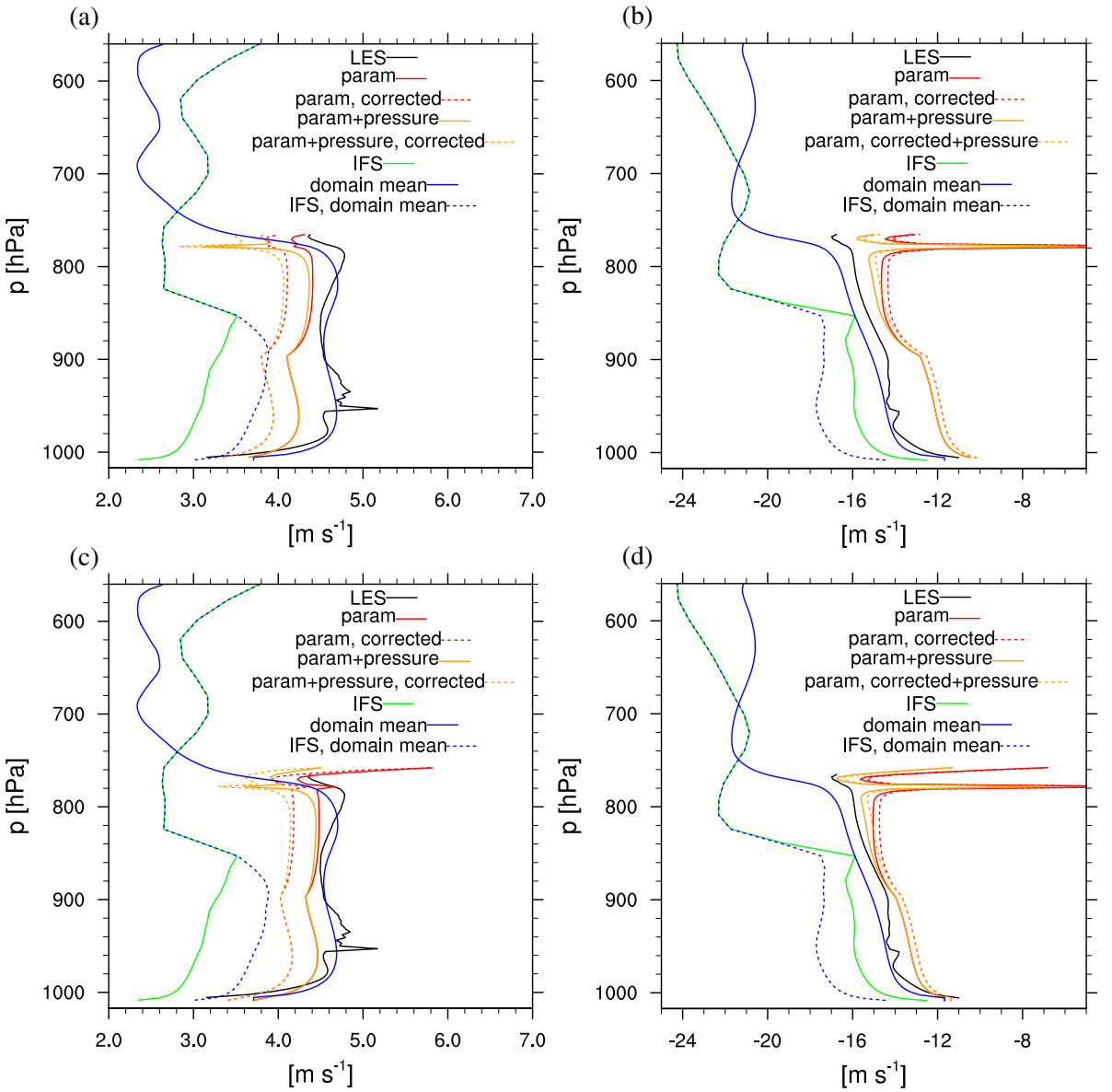


*Figure 19: In-cloud momentum as extracted from the LES (black solid), recalculated using LES values following the IFS routines (red), recalculated using LES values following the IFS routines and adding the pressure-gradient term (orange), values from the IFS (green), domain-mean values in the LES (solid blue) and environmental values in the IFS (dashed blue). The effect of applying the perturbation to the in-cloud values is illustrated by the dashed red and orange lines. (a) displays values for u, whereas (b) shows v. The impact of choosing the average value between cloud base and the departure level as cloud-base value (Eq. 9) to $u_u$ and $v_u$ is depicted in panels (c) and (d). Quantities are valid at 31 January 2010, 03 UTC.*

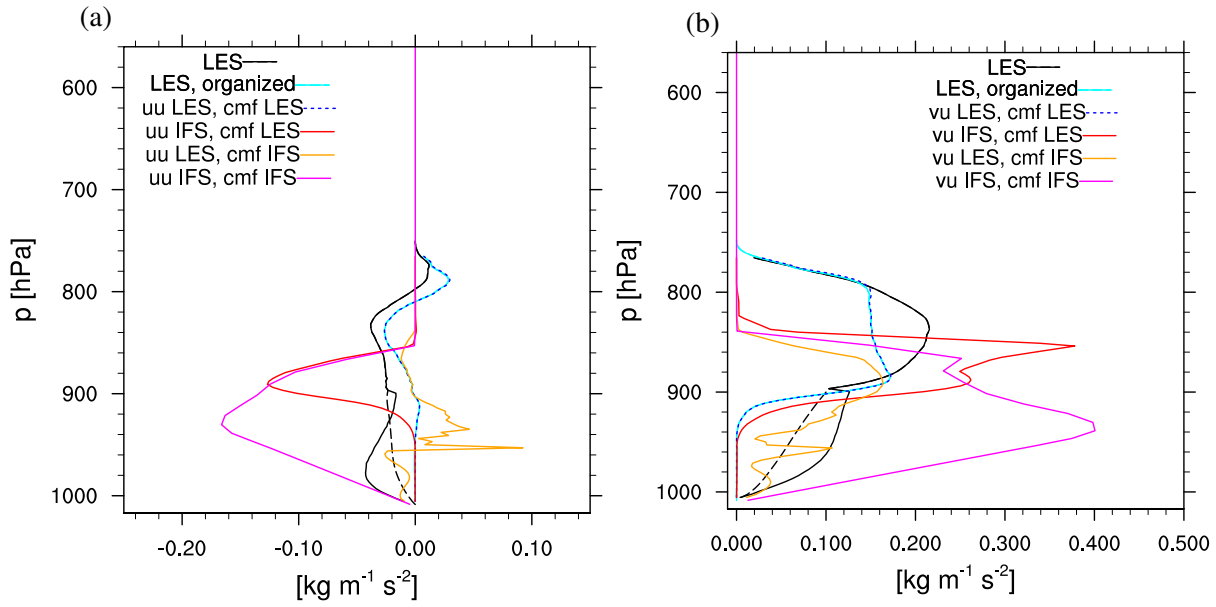


*Figure 20: Upward momentum flux (kg $m^{-1}$ $s^{-2}$) as extracted from the LES (black solid), the organised mass-flux term from the LES (cyan solid), recalculated using IFS values for $u_u$ but $M_u$ from the LES (red), recalculated using LES values for $u_u$ but $M_u$ from the IFS (orange) and values using both $u_u$ and $M_u$ from the IFS (magenta). (a) displays values for u, whereas (b) shows v.*

# 4 Conclusions

We have investigated the convective momentum transport and its representation in the IFS convection scheme for two different cases of shallow convection over ocean surfaces. The first case, RICO, shows considerable organisation of the cloud field over the course of the simulation. Even though the spatial cloud pattern changes markedly with the organisation, the characteristics of the momentum flux change little. The second case, CONSTRAIN, displays the deepening and breakup of stratocumulus clouds developing within strong wind shear in a cold-air outbreak. In both cases the momentum flux is down gradient and the flux divergence considerable, amounting to net accelerations of $2.5\,\mathrm{m\,s^{-1}\,h^{-1}}$.

We have dissected the terms entering the parametrisation of the momentum flux. The individual contributors from the IFS and the SCM version of the IFS are then compared to LES data. We have also integrated offline the IFS in-cloud momentum equations using LES data. A satisfactory representation of entrainment and detrainment yields an appropriate representation of the convective mass-flux profile. Yet, the value of cloud-base convective mass flux gauges the magnitude of the entire mass-flux profile and tends to be overestimated in the investigated cases. In-cloud momentum is the most critical quantity at the moment, an improvement of its representation could be beneficial for the entire convective momentum transport. While the parametrisations yields a decent shape of the vertical profile, assigning the value for in-cloud momentum at cloud base is crucial, as it sets the magnitude of the entire profile. Cloud-base values for in-cloud momentum proved to be underestimated in some cases, but overestimated in other instances. Thus, the correction term works successfully in some cases, while it worsens results in other cases. Moreover, we propose a new formulation for the correction term that eliminates a discontinuity that is present in the current formulation. A formulation for the correction term that uses the background wind between the departure level and the cloud base for cloud-base values shows promising results but still needs to demonstrate improvements on the global scale.

Including the pressure gradient across updraughts into the prediction for in-cloud momentum improves the shape of vertical profile of $u_u$ and $v_u$. Thus, it could be worthwhile to implement any of the discussed methods for parametrising it and check the impact onto the overall model performance. Yet, the pressure-gradient term does not capture the entire residuum between the divergence of the momentum flux and the entraining plume model. Using the mass-flux approximation to deduce the momentum flux introduces errors of similar order of magnitude as neglecting the pressure-gradient term.

While momentum flux is directed down-gradient in the current study, it would be interesting to further consider a case with counter-gradient momentum flux, in which CMT accelerates the mean flow. It is however not clear, how often these flow situations occur and how much they feed back onto the larger scales.

## Acknowledgements

We would like to thank Axel Seifert for providing the LES data for the RICO case and Lorenzo Tomassini for giving insight into the CONSTRAIN simulations. Moreover, we would like to thank Richard Forbes and Anton Beljaars for fruitful discussions on the study.

## References


Arakawa, A., and W. H. Schubert, 1974: Interaction of a Cumulus Cloud Ensemble with the Large-Scale Environment, Part I. *J. Atmos. Sci.*, **31 (3)**, 674–701, doi:10.1175/1520-0469(1974)031⟨0674:IOACCE⟩2.0.CO;2.

Brown, A., 1999: Large-Eddy Simulation and Parametrization of the Effects of Shear on Shallow Cumulus Convection. *Boundary-Layer Meteorology*, **91 (1)**, 65–80, doi:10.1023/A:1001836612775.

Brümmer, B., and S. Pohlmann, 2000: Wintertime roll and cell convection over Greenland and Barents Sea regions: A climatology. *Journal of Geophysical Research: Atmospheres*, **105 (D12)**, 15 559–15 566.

Carr, M. T., and C. S. Bretherton, 2001: Convective Momentum Transport over the Tropical Pacific: Budget Estimates. *J. Atmos. Sci.*, **58 (13)**, 1673–1693, doi:10.1175/1520.

de Rooy, W. C., and Coauthors, 2012: Entrainment and detrainment in cumulus convection: an overview. *Quart. J. Roy. Meteor. Soc.*, n/a–n/a, doi:10.1002/qj.1959.

Field, P. R., R. J. Cotton, K. McBeath, A. P. Lock, S. Webster, and R. P. Allan, 2014: Improving a convection-permitting model simulation of a cold air outbreak. *Quarterly Journal of the Royal Meteorological Society*, **140 (678)**, 124–138, doi:10.1002/qj.2116, URL http://dx.doi.org/10.1002/qj.2116.

Fu, Q., and K. N. Liou, 1993: Parameterization of the Radiative Properties of Cirrus Clouds. *J. Atmos. Sci*, **50 (13)**, 2008–2025.

Gregory, D., R. Kershaw, and P. M. Inness, 1997: Parametrization of momentum transport by convection. II: Tests in single-column and general circulation models. *Quarterly Journal of the Royal Meteorological Society*, **123 (541)**, 1153–1183, doi:10.1002/qj.49712354103, URL http://dx.doi.org/10.1002/qj.49712354103.

Gregory, D., and M. J. Miller, 1989: A numerical study of the parametrization of deep tropical convection. *Quarterly Journal of the Royal Meteorological Society*, **115 (490)**, 1209–1241, doi:10.1002/qj.49711549003, URL http://dx.doi.org/10.1002/qj.49711549003.

Grubišić, V., and M. W. Moncrieff, 2000: Parameterization of Convective Momentum Transport in Highly Baroclinic Conditions. *J. Atmos. Sci.*, **57 (18)**, 3035–3049, doi:10.1175/1520.

Hogan, T. F., and R. L. Pauley, 2007: The Impact of Convective Momentum Transport on Tropical Cyclone Track Forecasts Using the Emanuel Cumulus Parameterization. *Monthly Weather Review*, **135 (4)**, 1195–1207, doi:10.1175/MWR3365.1.

Inness, P. M., and D. Gregory, 1997: Aspects of the intraseasonal oscillation simulated by the hadley centre atmosphere model. *Climate Dynamics*, **13 (6)**, 441–458, doi:10.1007/s003820050176, URL http://dx.doi.org/10.1007/s003820050176.

Kershaw, R., and D. Gregory, 1997: Parametrization of momentum transport by convection. I: Theory and cloud modelling results. *Quarterly Journal of the Royal Meteorological Society*, **123 (541)**, 1133–1151, doi:10.1002/qj.49712354102, URL http://dx.doi.org/10.1002/qj.49712354102.

LeMone, M. A., 1983: Momentum Transport by a Line of Cumulonimbus. *J. Atmos. Sci.*, **40 (7)**, 1815–1834, doi:10.1175/1520.

Nowlin Jr., W. D., and C. A. Parker, 1974: Effects of a Cold-Air Outbreak on Shelf Waters of the Gulf of Mexico. *Journal of Physical Oceanography*, **4 (3)**, 467–486.

Pincus, R., and B. Stevens, 2009: Monte Carlo Spectral Integration: a Consistent Approximation for Radiative Transfer in Large Eddy Simulations. *Journal of Advances in Modeling Earth Systems*, **1 (1)**, 9 pp., doi:10.3894/JAMES.2009.1.1.

Schneider, E. K., and R. S. Lindzen, 1976: A discussion of the parameterization of momentum exchange by cumulus convection. *Journal of Geophysical Research*, **81 (18)**, 3158–3160, doi:10.1029/JC081i018p03158, URL http://dx.doi.org/10.1029/JC081i018p03158.

Seifert, A., and K. D. Beheng, 2001: A double-moment parameterization for simulating autoconversion, accretion and selfcollection. *Atmos. Res.*, **59–60**, 265–281.

Seifert, A., and K. D. Beheng, 2006: A two-moment cloud microphysics parameterization for mixed-phase clouds. Part 1: Model description. *Meteorol Atmos Phys*, **92**, 45–66.

Seifert, A., T. Heus, R. Pincus, and B. Stevens, 2015: Large-eddy simulation of the transient and near-equilibrium behavior of precipitating shallow convection. *Journal of Advances in Modeling Earth Systems*, n/a–n/a, doi:10.1002/2015MS000489, URL http://dx.doi.org/10.1002/2015MS000489.

Stevens, B., and A. Seifert, 2008: Understanding macrophysical outcomes of microphysical choices in simluations of shallow cumulus convection. *J. Met. Soc. Jap.*, **86**, 143–162.

Stevens, B., and Coauthors, 2005: Evaluation of Large-Eddy Simulations via Observations of Nocturnal Marine Stratocumulus. *Mon. Wea. Rev.*, **133 (6)**, 1443–1462.

Tiedtke, M., 1989: A comprehensive mass flux scheme for cumulus parameterization in large-scale models. *Mon. Wea. Rev.*, **117**, 1779–1800.

Tung, W., and M. Yanai, 2002a: Convective Momentum Transport Observed during the TOGA COARE IOP. Part I: General Features. *J. Atmos. Sci.*, **59 (11)**, 1857–1871, doi:10.1175/1520.

Tung, W., and M. Yanai, 2002b: Convective Momentum Transport Observed during the TOGA COARE IOP. Part II: Case Studies. *J. Atmos. Sci.*, **59 (17)**, 2535–2549, doi:10.1175/1520.

vanZanten, M. C., and Coauthors, 2011: Controls on precipitation and cloudiness in simulations of trade-wind cumulus as observed during rico. *Journal of Advances in Modeling Earth Systems*, **3 (2)**, 1–19, doi:10.1029/2011MS000056, URL http://dx.doi.org/10.1029/2011MS000056, m06001.

Wu, X., L. Deng, X. Song, and G. J. Zhang, 2007: Coupling of Convective Momentum Transport with Convective Heating in Global Climate Simulations. *J. Atmos. Sci.*, **64 (4)**, 1334–1349, doi:10.1175/JAS3894.1.

Zhang, G. J., and H.-R. Cho, 1991: Parameterization of the Vertical Transport of Momentum by Cumulus Clouds. Part I: Theory. *Journal of the Atmospheric Sciences*, **48 (12)**, 1483–1492, doi:10.1175/1520-0469(1991)048⟨1483:POTVTO⟩2.0.CO;2.

Zhang, G. J., and N. A. McFarlane, 1995: Role of convective scale momentum transport in climate simulation. *Journal of Geophysical Research: Atmospheres*, **100 (D1)**, 1417–1426, doi:10.1029/94JD02519, URL http://dx.doi.org/10.1029/94JD02519.

Zhang, G. J., and X. Wu, 2003: Convective Momentum Transport and Perturbation Pressure Field from a Cloud-Resolving Model Simulation. *J. Atmos. Sci.*, **60 (9)**, 1120–1139, doi:10.1175/1520.

Zhu, P., 2015: On the Mass-Flux Representation of Vertical Transport in Moist Convection. *Journal of the Atmospheric Sciences*, **72 (12)**, 4445–4468.